UNIVERSITY OF THESSALY

SCHOOL OF ENGINEERING

DEPARTMENT OF ELECTRICAL AND COMPUTER ENGINEERING

Obfuscation of Human Wireless micro-Doppler Signatures for Preventing Passive Human Activity Classification

Diploma Thesis

Margarita Loupa

Supervisor: Antonios Argyriou

June 2023

UNIVERSITY OF THESSALY

SCHOOL OF ENGINEERING

DEPARTMENT OF ELECTRICAL AND COMPUTER ENGINEERING

Obfuscation of Human Wireless micro-Doppler Signatures for Preventing Passive Human Activity Classification

Diploma Thesis

Margarita Loupa

Supervisor: Antonios Argyriou

June 2023

ΠΑΝΕΠΙΣΤΗΜΙΟ ΘΕΣΣΑΛΙΑΣ

ΠΟΛΥΤΕΧΝΙΚΗ ΣΧΟΛΗ

ΤΜΗΜΑ ΗΛΕΚΤΡΟΛΟΓΩΝ ΜΗΧΑΝΙΚΩΝ ΚΑΙ ΜΗΧΑΝΙΚΩΝ ΥΠΟΛΟΓΙΣΤΩΝ

Απόκρυψη ανθρώπινης δραστηριότητας από παθητικούς δέκτες μέσω αλλοίωσης κυματομορφών RADAR

Διπλωματική Εργασία

Μαργαρίτα Λούπα

Επιβλέπων: Αντώνιος Αργυρίου

Ιούνιος 2023

Approved by the Examination Committee:

Supervisor **Antonios Argyriou**
Associate Professor, Department of Electrical and Computer Engineering, University of Thessaly

Member **Dimitrios Bargiotas**
Professor, Department of Electrical and Computer Engineering, University of Thessaly

Member **Gerasimos Potamianos**
Associate Professor, Department of Electrical and Computer Engineering, University of Thessaly

Acknowledgements

I would like to express my sincere gratitude and appreciation to all those who have supported me throughout this thesis journey. Their guidance, encouragement, and unwavering support have been invaluable in the completion of this work.

First and foremost, I am deeply grateful to my supervisor, Dr. Antonios Argyriou. His expertise, patience, and dedication to teaching have shaped my research skills and fostered my academic growth. I am grateful for his mentorship and the countless hours he has dedicated to review and provide constructive feedback on my work. His insights and suggestions have significantly enhanced the quality of this thesis.

I would like to extend my heartfelt thanks to the members of the examination committee, Dr. Dimitrios Bargiotas and Dr. Gerasimos Potamianos. Their expertise and critical insights have greatly enriched my research. I am grateful for their time, commitment, and thorough examination of this thesis.

I am also grateful to my beloved family and friends for their unconditional love, encouragement, and endless support during the countless hours I spent studying and working on this thesis.

Lastly, I want to express my gratitude to all the individuals, both known and unknown, who have contributed to my academic journey in any way. Your influence, encouragement, and inspiration have played a significant role in my growth as a scholar.

DISCLAIMER ON ACADEMIC ETHICS AND INTELLECTUAL PROPERTY RIGHTS

«Being fully aware of the implications of copyright laws, I expressly state that this diploma thesis, as well as the electronic files and source codes developed or modified in the course of this thesis, are solely the product of my personal work and do not infringe any rights of intellectual property, personality and personal data of third parties, do not contain work / contributions of third parties for which the permission of the authors / beneficiaries is required and are not a product of partial or complete plagiarism, while the sources used are limited to the bibliographic references only and meet the rules of scientific citing. The points where I have used ideas, text, files and / or sources of other authors are clearly mentioned in the text with the appropriate citation and the relevant complete reference is included in the bibliographic references section. I also declare that the results of the work have not been used to obtain another degree. I fully, individually and personally undertake all legal and administrative consequences that may arise in the event that it is proven, in the course of time, that this thesis or part of it does not belong to me because it is a product of plagiarism».

The declarant

Margarita Loupa

Diploma Thesis

Obfuscation of Human Wireless micro-Doppler Signatures for Preventing Passive Human Activity Classification

Margarita Loupa

Abstract

Human activity recognition based on micro-Doppler signatures is a popular and an active area of research. When a wireless radar waveform reflects off of a moving target, the resulting reflected signal exhibits distinct frequency shifts, caused by the motion of the target. A receiver can leverage these shifts to generate their corresponding spectrograms, thereby producing the micro-Doppler signatures associated with the target's identity and activity. However, due to the nature of the wireless channel, unauthorized receivers can also intercept the reflected signal and compute these spectrograms, consequently exposing the target's identity, which poses a significant privacy breach when the target remains unaware of it. To attend this issue, two techniques were investigated to obscure the micro-Doppler characteristics, aiming to impede their interpretation by malicious users. The first technique involved the injection of a frequency-varied signal into the transmitting radar waveform, effectively obfuscating the micro-Doppler signatures without disrupting the classification process in the authorized receiver. The second technique utilized a uniform linear array of 30 isotropic antennas, employing a specific pattern to activate and deactivate the array elements within specific time intervals. This approach effectively obscures the micro-Doppler signatures just by leveraging the inherent physical properties of the array, but it affects the classification process in the active radar to some extent. Both techniques were implemented and evaluated using Mathworks' MATLAB, testing them across five distinct scenarios that involved the presence of both pedestrians and bicyclists, using a monostatic radar configuration that utilized FMCW waveforms for transmission. By utilizing a pre-trained convolutional neural network on a large dataset, across all five scenarios, the results demonstrated that in both approaches, the Doppler signatures are successfully obfuscated. The first technique achieved to reduce the classification accuracy at 30.75%, while the second technique dropped it at 9%.

Keywords: human activity classification, deep learning, micro-Doppler, passive radars

Διπλωματική Εργασία

Απόκρυψη ανθρώπινης δραστηριότητας από παθητικούς δέκτες μέσω αλλοίωσης κυματομορφών RADAR

Μαργαρίτα Λούπα

Περίληψη

Η αναγνώριση ανθρώπινης δραστηριότητας βασισμένη στα micro-Doppler χαρακτηριστικά είναι ένα δημοφιλές και ενεργό πεδίο έρευνας. Όταν ένα ασύρματο σήμα ραντάρ ανακλάται από έναν κινούμενο στόχο, τότε το ανακλώμενο σήμα περιέχει διάφορες μετατοπίσεις Doppler. Ένας δέκτης μπορεί να εκμεταλλετεί αυτές τις μετατοπίσεις και να δημιουργήσει τα αντίστοιχα φασματογράμματα, έτσι ώστε να παράξει υπογραφές Doppler που θα αποκαλύπτουν την ταυτότητα και την δραστηριότητα του στόχου. Παρόλα αυτά, λόγω της φύσης ενός ασύρματου καναλιού, κάποιος μη εξουσιοδοτημένος δέκτης μπορεί να υποκλέψει την ανακλώμενη ακτινοβολία του στόχου και να παράξει ο ίδιος τα αντίστοιχα φασματογράμματα, αναγνωρίζοντας έτσι τον στόχο. Κάτι τέτοιο αποτελεί παραβίαση των προσωπικών δεδομένων του στόχου, αν ο ίδιος δεν γνωρίζει για την δραστηριότητα αυτή. Για να αντιμετωπιστεί αυτό το θέμα, διερευνήθηκαν δύο τεχνικές που μπορούν με επιτυχία να αλλοιώσουν τις κυματομορφές ραντάρ, έτσι ώστε οι παραγόμενες υπογραφές των στόχων να μην μπορούν να αναγνωριστούν από κάποιον κακόβουλο χρήστη. Η πρώτη τεχνική περιλαμβάνει την προσθήκη ενός σήματος μεταβαλλόμενης συχνότητας στην μεταδιδόμενη κυματομορφή, έτσι ώστε να αλλοιώσει τις προαναφερθέντες υπογραφές χωρίς να επηρεαστεί η διαδικασία αναγνώρισης του στόχου στο εξουσιοδοτημένο ραντάρ, αν αυτή χρειάζεται. Η δεύτερη τεχνική χρησιμοποιεί μια συστοιχία από 30 γραμμικά τοποθετημένες, ομοιόμορφες, ισοτροπικές κεραίες, όπου κάθε κεραία ενεργοποιείται και απενεργοποιείται με συγκεκριμένο μοτίβο και σε συγκεκριμένο χρόνο διάστημα. Η δεύτερη προσέγγιση καταφέρνει να αλλοιώσει τις υπογραφές Doppler, απλά εκμεταλλευόμενη των φυσικών χαρακτηριστικών της συστοιχίας. Παρόλα αυτά, η συγκεκριμένη μέθοδος επηρεάζει την διαδικασία ταυτοποίησης των στόχων και στο ενεργό ραντάρ κατά έναν βαθμό. Και οι δύο τεχνικές υλοποίηθηκαν και αξιολογήθηκαν χρησιμοποιώντας την εφαρμογή MATLAB της Mathworks, μέσα από πέντε διαφορετικά σενάρια, που περιλάμβαναν την παρουσία τόσο πεζών όσο και ποδηλατών. Στον προσωμοιωτή χρησιμοποιήθηκε ένα μονοστατικό ραντάρ που εξέπεμπε FMCW κυματομορφές. Χρησιμο-

ποιώντας ένα ήδη εκπαιδευμένο συνελικτικό νευρωνικό δίκτυο πάνω σε έναν μεγάλο αριθμό δειγμάτων, και για τα πέντε σενάρια, τα αποτελέσματα έδειξαν πως είναι δυνατή η αλλοίωση κυματομορφών ραντάρ και στις δύο περιπτώσεις, αποκρύπτοντας έτσι την ανθρώπινη δραστηριότητα από το παθητικό ραντάρ. Η πρώτη τεχνική κατάφερε να ρίξει την ακρίβεια κατηγοριοποίησης των στόχων στο 30.75%, ενώ η δεύτερη τεχνική στο 9%.

Λέξεις-κλειδιά: αναγνώριση ανθρώπινης δραστηριότητας, βαθειά μάθηση, micro-Doppler, παθητικά ραντάρ

Table of contents

List of figures

List of tables

Abbreviations

6G	Sixth Generation
ADS	Automatic Detection System
AOA	Angle of Arrival
BW	Bandwidth
CFAR	Constant False Alarm Rate
CH	Chain Home
CHL	Chain Home Low
CNN	Convolutional Neural Network
CFR	Channel Frequency Response
CSSAD	Committee for the Scientific Survey of Air Defense
CSI	Channel State Information
CW	Continuous Wave
DL	Deep Learning
DNN	Deep Neural Network
DOA	Direction of Arrival
FFT	Fast Fourier Transform
FMCW	Frequency Modulated Continuous Waveform
FM	Frequency Modulated
G	Gain
IF	Intermediate Frequency
I	In-Phase
JRC	Joint Radar Communication
LFM	Linear Frequency Modulation
LLRT	Log-Likelihood Ratio Test
LNA	Low Noise Amplifier

LRT	Likelihood Ratio Test
MVDR	Minimum Variance Distortionless Response
MF	Matched Filter
ML	Machine Learning
MTI	Moving Target Indicator
NP	Neyman-Pearson
PRI	Pulse Repetition Interval
Q	Quadrature
QTFD	Quadratic Time-Frequency Distribution
RADAR	Radio Detection and Ranging
RCS	Radar Cross Section
ReLU	Rectified Linear Unit
RF	Radio Frequency
SAR	Synthetic Aperture Radar
SNR	Signal to Noise Ratio
STAP	Space-Time Adaptive Processing
STFT	Short Time Fourier Transform
TF	Time-Frequency
ULA	Uniform Linear Array

Chapter 1

Introduction

Over the past decades, radar technology has experienced remarkable progress, evolving from its conceptualization in the late 19th century, as a means to detect targets at specific distances, to its current application across various domains. Today, radar technology finds utility in diverse fields, that include weather forecasting, remote sensing, military operations, space exploration, and as well as residential applications.

As we approach the era of sixth-generation technology (6G) [1], the integration of radars into the communications' infrastructure promises to merge communication, networking, and artificial intelligence capabilities into a joint radar-communication system (JRC) [2]. One intriguing aspect of this system, that has already emerged, is the use of radar waveforms for sensing human movement and activity, enabling the development of applications for smart homes and devices that leverage the radar's inherent sensing capabilities. Such applications involve Human Activity Recognition [3], Vital Sign Monitoring [4], Gesture Recognition [5], as well as Security and Defense Applications [6], all rooted in the fundamental concept of detecting and analyzing human motion. However, while these advancements hold great potential for improving the quality of life, concerns regarding privacy violations loom large, necessitating careful consideration and investigation.

1.1 Thesis Scope

In the context of radar sensing, when a transmitting waveform propagates into a wireless channel and interacts with a moving target, then the reflected echoes contain micro-frequency fluctuations, caused by the target's motions. These fluctuations can be properly extracted

through the application of a time-frequency analysis, which produces distinct patterns that are indicative of specific target movements, commonly known as as micro-Doppler signatures. Various classification algorithms have been developed, to accurately categorize these signatures. However, due to the nature of the channel, unauthorized users can intercept these echoes and analyze their patterns, thereby breaching the privacy of individuals who remain oblivious to such interception.

The objective of this thesis is to investigate effective techniques, aimed at obfuscating micro-Doppler characteristics, preventing their interpretation by unauthorized users. In Chapter 5, Mathworks' MATLAB application was utilized to create a simulated environment and generate the necessary data for testing these methods. Two obfuscation techniques were examined within five diverse scenarios: a single moving pedestrian, a single moving bicyclist, two moving pedestrians, two moving bicyclists, and the concurrent presence of a moving pedestrian and bicyclist in the same scene.

1. The first technique involved applying a frequency variated signal to the transmitting waveform, without disrupting the demodulation process at the authorized receiver. The impinged signal distorts the extracted signatures, thus making them unrecognizable for classification at the unauthorized receiver.

2. The second technique employed a phased array system, strategically toggling the activation and deactivation of specific elements. This resulted in tampering the produced signatures of the objected target to a certain degree, thereby making the classification process very challenging. This approach impacts the authorized receiver to some extent as well.

1.1.1 Contribution

The contribution of this thesis is summarized as follows:

1. A comprehensive review was conducted on radar theory and its applications in deep learning.

2. Two simulations were implemented in the MATLAB environment to model the transmission and reception of signals in a monostatic radar system. Both simulations involved performing time-frequency analysis on the received signals and applying a

trained Convolutional Neural Network for classification. The first simulation utilized a single antenna for signal transmission, while the second simulation employed a phased array configuration.

3. The obfuscation techniques discussed earlier were implemented individually, and their results were analyzed and compared.

1.2 Volume Structure

This thesis is structured into five chapters, each designed to provide the reader with the necessary knowledge to progress to the next chapter. Chapter 2 offers a comprehensive exploration of radar, tracing its historical evolution and examining its diverse modern applications. Chapter 3 establishes the foundational theoretical framework of radar, which serves as the basis for the case study in this thesis. In Chapter 4, Convolutional Neural Networks are extensively reviewed, focusing on the fundamental components commonly utilized in classification tasks. Chapter 5 presents the detailed analysis of the case study, addressing the central problem of the thesis and exploring two distinct techniques to solve it. Lastly, Chapter 6 presents the findings of the case study and discusses potential future improvements.

Chapter 2

Radar History and Applications

2.1 Introduction

This chapter provides a comprehensive exploration of the essence of radar, delving into its historical evolution, from its inception as an idea in the late 19th century, to its pivotal advancements during World War II, and ultimately, it sheds light on the modern radar's applications, offering a glimpse into the expansive array of operations and functions for which radars are utilized in the modern era.

2.2 Meaning and Significance of Radar

Originally, *radar* was an acronym for "RAdio Detection And Ranging", a term that was coined in 1939 [7] by the United States Army Signal Corps. However, in modern times, the technology has become so prevalent that the term has transitioned from an acronym to a commonly used noun in English language. A radar, is an electromagnetic system that uses radio waves to detect, locate, and track objects. This system functions by transmitting electromagnetic radiation into space and subsequently analyzing the echo signals, reflected back from an object or target. This provides valuable information regarding the object's distance, angle, and velocity, in relation to the radar site. Compared to other sensing technologies, radars possess significant advantages, due to their ability to operate efficiently over both short and long distances, and in challenging conditions. These include scenarios with poor visibility due to darkness, fog, rain, or snow, as well as situations where the object is obscured by other factors, such as vegetation or terrain. Additionally, radars can penetrate non-conductive ma-

terials, such as walls, to detect and locate objects on the other side.

The versatility of a radar makes it an indispensable tool for both military and civilian applications, owing to its exceptional capability to identify and monitor a diverse range of objects such as airplanes, vessels, missiles, automobiles, meteorological patterns, and even humans.

2.3 Historical Overview

The origins of radars [8, 9] can be traced back to the experiments conducted by Heinrich Hertz in the late 19th century. He used an apparatus, similar to a modern-day pulse radar, which operated at frequencies in the vicinity of 455 MHz. His observations provided experimental evidence for James Clerk Maxwell's theory on electromagnetism, since he confirmed that radio waves exhibited similar characteristics to light, but with some variations in the frequencies between them. During his experiments, Hertz discovered that radio waves were reflected by metallic objects, but he further noticed that nearby objects also interfered with the reflected waves. Around the turn of the century, scientists became aware of this phenomenon and began to consider how to utilize it. In 1900, Nikola Tesla proposed a wireless system that would employ the reflected radio waves to detect and locate objects, even measuring their distance, but his ideas were dismissed at that time.

In the early 20th century, the German inventor Christian Hülsmeyer developed the *Telemobiloscope* [9, 10], a simple naval detection device that utilized radio echoes to remotely detect ships and other nearby objects, as a means to help preventing collisions in foggy conditions. The *Telemobiloscope* consisted of a spark-gap transmitter, connected to an array of dipole antennas, and a coherer receiver with a rotating cylindrical parabolic antenna that could detect reflected signals up to 3 km away. Although the device did not initially provide range information, Hülsmeyer patented a method in 1906 that used two vertical measurements and trigonometry to calculate approximate range. During bad weather, the device would be periodically spun to check for nearby ships and, upon detecting a reflected signal, it would activate a relay that rang an electric bell to alert for objects in close proximity.

In the 1930s, eight countries [7] with existing radio technology and military concerns, independently and almost concurrently began efforts to utilize radio echoes for aircraft detection. These countries included the United States, Great Britain, Germany, France, the Soviet

Union, Italy, the Netherlands, and Japan, each embarking on the development of radar with differing degrees of motivation and success. As a result, several of these countries had some operational radar equipment in military service by the onset of World War II.

Dr. Rudolph Kühnold, who led the German Navy's signals research in the 1930s, was studying ways to detect underwater objects using sound waves. He realized that the same principles could be applied to radio waves above water and, with the help of amateur radio operators Paul-Günther Erbslöh and Hans-Karl Freiherr von Willisen, founded the company "Gesellschaft für Elektroakustische und Mechanische Apparate" (GEMA) to develop a radio measuring device for research. GEMA's team focused on creating a high resolution radar and, after several successful attempts, they extended the device's range up to 80 km by the end of 1936. The radar, named *Freya*, became the most important early-warning radar for German aircrafts and ships in 1938. GEMA also developed a short-range gun ranging radar called *Seetakt*, which worked at an even higher frequency than *Freya*. Later, the Telefunken company also became interested in radars, right after GEMA started securing significant military contracts. Telefunken went on to create a small and mobile radar called *Würzburg*, which could plot aircrafts with high accuracy, up to 40 km away.

Even though the German industry had initially focused on naval surface radars, it inadvertently set the foundations for modern air defense systems. The remarkable technological advancements in radar technology during this period also played a crucial role in the progress of World War II and beyond.

In Britain, the possibility of air raids and the potential of invasion by air and sea, due to the impending World War II, prompted a significant push towards building specialized defence systems. To address this, in November 1934, the Air Ministry of Britain created the "Committee for the Scientific Survey of Air Defense" (CSSAD), also known as the "Tizard committee". Its primary responsibility was to evaluate the employment of recent developments in the scientific and technical field, so that to enhance current defense strategies against hostile attacks.

During 1935, Sir Robert Watson Watt, A. F. Wilkins and H. E. Wimperis, along with Sir Henry Tizard, contributed to the development of a radar system that is now known as *Chain Home* (CH). In 1937, the Bawdsey Research Station constructed a prototype CH station that was later transferred to the Royal Air Force. The CH station operated at a frequency of 22 MHz, and in favorable weather conditions, it could detect aircraft flying up to 150 km away

at an altitude of 3 km. By September 1939, 20 CH stations were in operation, and they were employed in the Battle of Britain. While the CH had some limitations, such as an elevation limit and an inability to detect low-flying aircraft, it was a resounding success.

Afterwards, in 1937, a beamed radar for airborne and coastal defense was developed, known as the *Chain Home Low* (CHL) radar. The CHL operated at 200MHz, had an antenna that rotated at 1-2.3 rpm and a range of 160 km, with an azimuth accuracy of 1.5 degrees. The duration of the pulse was adjustable between 5 and 25 μs, with a selectable repetition rate as either 25 or 50 Hz. Unfortunately, it could not determine height, and only 11 CHLs were operational by 1941.

However, the ability to generate short pulses of radio energy was a crucial breakthrough that enabled the emergence of modern radar systems. By timing the pulses on an oscilloscope, the range could be determined, and the antenna's direction could reveal the angular location of targets. The combination of these two pieces of information produced a "fix", enabling the target's relative position to be located. *Chain Home* was a significant milestone in the history of radar technology, and its development marked a turning point in the use of radars.

In the United States, during the same time period, the groundwork for the development of a pulsed radar system was established, thanks to the contributions of the engineers Albert H. Taylor, Leo C. Young, Lawrence A. Hyland and of the physicist Robert Morris Page. While carrying out communication experiments at the U.S. Naval Aircraft Radio Laboratory in 1922, Taylor and Young noticed that while a wooden ship was passing through the Potomac river, it was interfering with their experiments. Based on this observation, they suggested employing a system for detecting ships in harbor defense (which shared a configuration similar to today's bistatic radars), but their idea was rejected. However, in 1930, Lawrence A. Hyland, who was working with Taylor and Young at the U.S. Naval Research Laboratory, detected a passing aircraft using a similar radio configuration. This achievement led to a proposal and patent for the technique of interference to detect ships and aircrafts.

In 1924, Robert Morris Page was assigned to implement Young's suggestion of using pulsing techniques instead, to directly determine the range to the target. In December 1934, Page's transmitter design, operating at 60 MHz and pulsed for 10 μs with 90 μs between pulses, detected a plane flying up and down the Potomac river, from a distance of 1.6 km. This experiment demonstrated the fundamental concept of a pulsed radar system and is widely credited as the world's first true radar.

Page's invention of the duplexer device was also crucial for the development of radar technology, as it enabled the transmitter and receiver to share the same antenna, eliminating the risk of damaging the receiver circuitry. This innovation also resolved the issue of synchronizing separate transmitter and receiver antennas, which is essential for precise positioning of distant targets. Further experiments with pulsed radar resulted in a prototype radar system demonstrated to government officials in June 1936. Operating at 28.6 MHz, this radar system successfully tracked an aircraft at distances up to 40 km. However, due to the system's low-frequency signals, it required large antennas, making it impractical for mounting on ships or aircraft.

While the impetus for the early development of radar technology was military, the 20th century played a crucial role in advancing the research and development of this field. From the pioneering work of engineers and physicists such as Albert H. Taylor, Leo C. Young, Lawrence A. Hyland, and Robert Morris Page in the United States, to the breakthroughs achieved in other countries such as Britain and Germany, radar technology rapidly progressed from the initial detection of nearby ships and aircrafts, to accurate long-range tracking capabilities.

2.4 Modern Radar Applications

Today, radars are an essential tool used in various fields, ranging from weather forecasting to air traffic control, demonstrating the far-reaching impact of the pioneering research conducted in the early stages of radar development. Outlined below are brief descriptions [8, 11] of the primary domains in which radar technology finds widespread use:

Military: Modern radars are extensively employed in military operations due to their versatility and effectiveness. Capable of operating at different frequencies, military radars can detect various targets, from ground vehicles and aircraft to missiles and small drones. Consequently, they offer air-defense, early warning, weapon control, and ground surveillance capabilities, thus becoming an indispensable tool for defense forces around the world.

Remote Sensing: Remote sensing applications have extensively embraced the use of radars, which offer valuable insights into a plethora of environmental phenomena, including weather and planetary observations. With radar-based remote sensing, it is now feasible to detect and measure objects, or features, that are challenging or impossible to observe with traditional

sensors, such as cameras.

Air-Traffic Control: The safety of modern air travel can be attributed to the successful integration of radar technology in air traffic control. Major airports rely on surveillance radars to monitor air traffic and gather weather information in the surrounding area. These airports also utilize radar systems to oversee and manage aircraft and ground vehicle traffic on the runways, as well as en route traffic. Such systems are employed globally to ensure effective and secure air traffic control.

Space: Radar technology finds a broad range of applications in space. Synthetic Aperture Radar (SAR) is a specialized type of radar that can produce high-resolution images of the Earth's surface even in unfavorable weather conditions or at night. This technology is valuable for various purposes, including environmental monitoring, natural disaster tracking, and topography analysis. Planetary exploration missions also utilize radar systems to examine the surface of planets and moons in the solar system. In addition, radar systems can also be used to help monitoring and tracking space debris and other objects in orbit, providing crucial data to ensure the safety of spacecrafts and satellites.

Maritime Industry: Radar technology is an indispensable component of the maritime industry, as it provides ships with vital information to navigate through challenging conditions, such as reduced visibility due to fog, darkness, or adverse weather. By detecting and tracking other coastlines and navigational hazards, radar systems help in the prevention of accidents and disasters at sea. Moreover, radar systems assist ships in avoiding collisions with other vessels, thereby enhancing the safety of the crew and passengers onboard.

In conclusion, due to the ever-increasing advancements in this technology, the potential applications of radars continue to expand, making them an essential component of the modern world. As such, the study of radar technology is of critical importance for scientists and engineers, as it equips them with the expertise and skills required to create and implement pioneering solutions that can address the constantly evolving needs of society. In this way, the continuing exploration of radar technology promises to yield many more exciting and groundbreaking developments in the future.

Chapter 3

Radar Theory

3.1 Introduction

As previously explained in Chapter 2, radars are electromagnetic systems, designed to detect, locate, and monitor objects, through the use of transmitted electromagnetic radiation. By analyzing the echoes that are reflected back from targets within the radars' vicinity, these systems are able to extract valuable information about the target's range, velocity and location. This process enables radar technology to provide valuable insights and intelligence across a range of applications, from military surveillance to weather forecasting and beyond.

The ascent of radar technology and its widespread adoption across various aspects of life, including the military, urban environments, and even residential settings, has paved the way for an expansive array of applications. This has created opportunities to enhance security, safety, improve the quality of life, as well as effectively manage well-being. Looking ahead, the forthcoming sixth generation technology (6G) will introduce an innovative joint radar-communication system (JRC) [1], that will integrate radar sensing into the communication infrastructure. This integration holds immense potential, but also presents notable challenges. Given that radar sensing involves tracking and detecting movements, there is a concern regarding privacy violations if individuals being monitored are unaware of the surveillance. Hence, this thesis focuses on devising mechanisms to safeguard against any malicious attempts to extract information from individuals under radar surveillance.

This chapter provides the essential theoretical framework that will be applied in the case study of this thesis, accompanied by an adequate description of the signal processing techniques that are critical to the operation of radars, elucidating their most significant features

and functions. Through this comprehensive and in-depth analysis, readers will gain a robust understanding of the theoretical concepts and practical techniques that are essential to the successful design, implementation, and optimization of radar systems.

3.2 Monostatic Radar Model

A fundamental type of radar utilized in modern times is the *monostatic* radar. This type of configuration employs both the transmitting and receiving components of the radar system at the same location, utilizing a singular antenna on a time-shared basis to serve both functions. The co-location of the transmitter and receiver elements results in a significant reduction of the complexity of the radar system's hardware. This feature simplifies the system design and makes it more economical to construct and maintain, especially when compared to more complex configurations, such as bistatic and multistatic radars.

Figure 3.1 illustrates the operating principles of a monostatic radar, wherein, an electromagnetic signal is generated by a transmitter and is radiated through a single antenna into free space. When the signal encounters the target, a portion of it is absorbed, while the remaining energy is reflected back in a multitude of directions. Then, the same antenna captures some of the backscattered energy, which is subsequently delivered to the receiver for further processing.

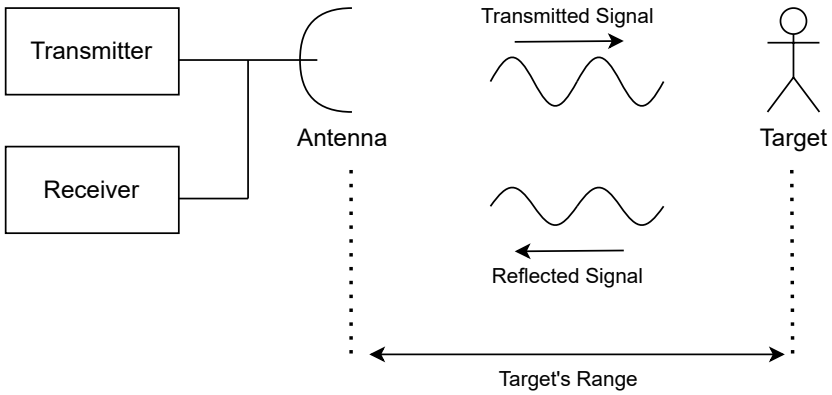

Figure 3.1: The operating principles of a monostatic radar system [8].

A much more exhaustive and comprehensive illustration of the operational mechanism of a monostatic radar [8, 12, 13, 14] can be portrayed in the form of a block diagram. Figure 3.2 offers a detailed depiction of the various components of a simple monostatic pulse radar and their respective arrangements within the configuration.

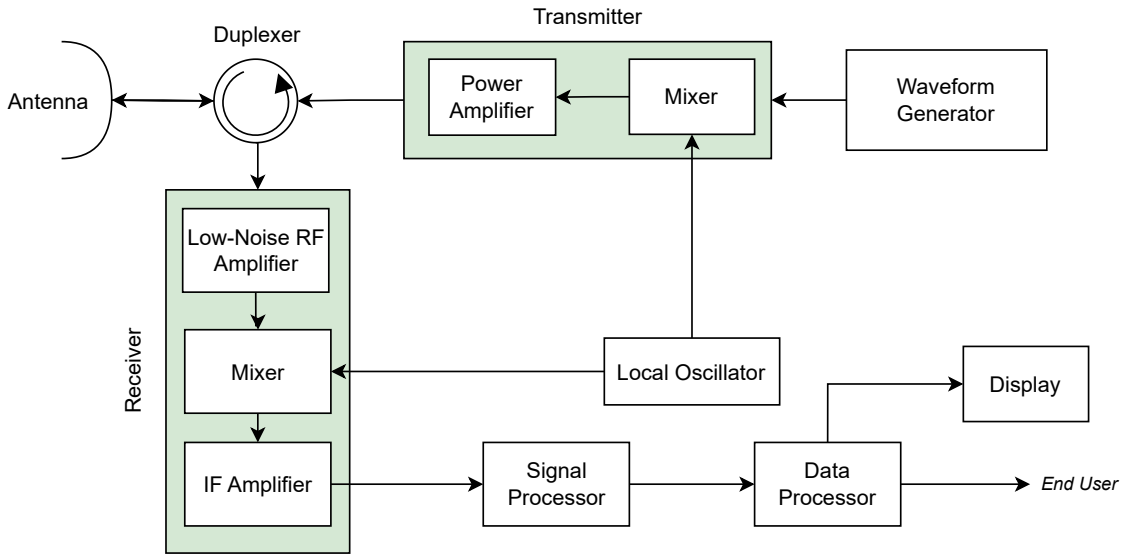

Figure 3.2: Block diagram of a simple monostatic pulse radar [12].

3.2.1 Transmission

The radar signal is first created through the use of a *waveform generator*, which generates a low-powered signal. In contemporary radar systems, this generator is typically a digital signal generator, capable of producing a diverse array of waveforms such as pulse and continuous wave signals. The selection of the waveform will be contingent on the particular application and the radar's intended performance characteristics.

The generated waveform undergoes modulation to the desired carrier radio frequency (RF) at the *mixer*, resulting in a modulated signal that is subsequently amplified to an appropriate level in the *power amplifier*. In radar systems, power amplifiers are typically of high-power, capable of providing tens to hundreds of Watts of power to the antenna. These amplifiers are engineered to function across a wide frequency range and exhibit a linear response to the input signal. The linearity of the amplifier is crucial in upholding the transmitted signal's integrity and in mitigating distortion and interference that may occur during transmission. Hence, this system governs the transmitted signal's strength, ultimately influencing the radar's maximum range and resolution. The selection of the amplifier technology and topology is predicated on the radar's frequency band, power requirements, and system constraints.

Following amplification, the signal is primed for transmission via a *waveguide* or a *transmission line* system, ultimately being radiated into space by a shared antenna. Waveguides are a specialized form of transmission line used in high-power radars, like weather radars and air

traffic control radars. They are hollow metallic tubes that guide electromagnetic waves with minimal loss, maximal power handling capacity and minimal distortion. In contrast, transmission lines are utilized for lower frequency signals and are typically employed in small to medium-sized radars. A transmission line comprises of a two-wire structure that facilitates the radio-frequency energy transmission from one location to another. The transmission line is utilized to match the impedance of the antenna to that of the transmitter or receiver, thereby ensuring optimal energy transfer efficiency. The design and selection of these two systems are predicated on the radar signal's frequency, power level, and desired efficiency of the radar system.

The *antenna* serves as the conduit for transmitting energy into space and then collecting echo energy during receive mode. Typically, the antenna is directive, capable of being mechanically or electronically steered to yield the desired directionality of the emitted signal. The antenna is frequently engineered to generate a narrow, directive beam during transmission, with a correspondingly large area during reception, enabling the detection of weak echo signals from the target. Furthermore, the antenna functions as a spatial filter, suppressing signals originating from other directions, such as interference or jamming signals.

Upon leaving the antenna, the radio frequency energy undergoes atmospheric refraction and attenuation. The energy will be scattered, and a portion of will be reflected back to the radar.

The utilization of a *duplexer* enables the antenna to perform both transmission and reception of signals in a time-shared basis, while also safeguarding the receiver from potential burnout. By allowing the antenna to switch between transmit and receive modes, the duplexer facilitates the transfer of signals between the radar system and the target object, with greater efficiency and accuracy.

3.2.2 Reception

In the receive mode, the radar system operates by gathering the weak echoes through the same antenna, then routing them via the duplexer to a *superheterodyne radar receiver*. A superheterodyne receiver, also known as a *superhet*, is a type of radio receiver that employs the mixing of a locally generated frequency with the carrier frequency, to produce an intermediate frequency (IF) signal, with a frequency that is lower than the original modulated one. The purpose of this frequency conversion is to facilitate the demodulation of the signal by

reducing it to a more manageable frequency.

In order to optimize the processing of the returned echoes, the receiver has to amplify them to a more suitable level. However, especially at microwave frequencies, the clutter caused by unwanted echoes from the environment is the most significant source of noise that affects a radar's performance. To address this issue, a *low-noise RF amplifier* (LNA) is utilized to amplify the faint radar signals received by the antenna before they reach the mixer, thereby reducing clutter noise. Yet, it is also crucial to minimize the amount of noise generated by the receiver itself and for that reason, the LNA is designed with an extremely low noise figure, which quantifies the amount of noise added to the signal by the amplifier. For this reason, the LNA helps to improve the sensitivity of the radar system, making it more effective at detecting targets in the presence of clutter noise, without disrupting the signal-to-noise ratio (SNR).

The RF signal is then directed to a circuit where it undergoes a *heterodyning* conversion, by mixing it with a sine wave signal that was generated by a variable frequency oscillator known as the *local oscillator* (LO). The LO and mixer work in tandem to down-convert the frequency of the received signal to an IF that is more convenient for subsequent processing. The LO provides a stable and tunable signal, close in frequency to the received RF signal, whereas the mixer is a non-linear component that multiplies the RF signal by the LO signal. The mixer produces a signal that includes the original RF signal at f_{RF}, the local oscillator signal at f_{LO}, as well as the sum and difference frequencies $f_{RF} + f_{LO}$ and $f_{RF} - f_{LO}$. To minimize the appearance of these frequencies, an *IF amplifier* is then used to amplify and filter the mixer's output signal. The use of modulation to IF rather than directly to baseband, results in a lower conversion loss, thereby enhancing the receiver's sensitivity.

The IF is designed with high gain, a narrow bandwidth, and low noise figure, making it ideal for amplifying and filtering the weak IF signals produced by the mixer. Acting as a matched filter (MF), its bandwidth is aligned with the pulse width of the transmitted radar signal, allowing for optimal signal amplification and processing, while simultaneously reducing out-of-band noise and interference. Additionally, to minimize the effects of flicker noise, also known as *pink noise*, most receivers integrate an extra IF amplification stage. The IF amplifier's ability to filter out unwanted noise and interference enhances the radar system's capability to extract useful information from the received signal, resulting in improved detection and tracking performance. Once the signal is amplified, it is then demodulated to

baseband for further processing.

After passing through the IF amplifier, the baseband signal is directed to the *signal processor*, a critical component of radar systems that plays a vital role in extracting and analyzing relevant information from the received signal. The signal processor performs advanced mathematical and digital signal processing techniques to filter out unwanted noise and interference, allowing it to isolate the desired signal and improve the accuracy of the detection process.

An excellent example of a signal processing technique is *Doppler Filtering*. This technique is used to separate the desired moving targets from undesired stationary clutter echoes, which can be a significant source of noise and interference in radar systems. The *Doppler effect* causes the frequency of the radar echoes from moving targets to shift, and Doppler Filtering takes advantage of this effect to distinguish between moving targets and stationary clutter. By applying a filter to the received signal that only allows frequencies within a certain range (corresponding to the expected Doppler shift of moving targets) to pass through, Doppler Filtering effectively removes unwanted clutter and enhances the radar's ability to detect and track moving targets.

After the received signal has been processed, a decision is made on the presence or absence of a target. If a target is detected, some radar systems may use a *data processor* to perform additional processing before displaying the information. One example of such a processor is the Automatic Detection and Tracking System (ADS), which performs a variety of functions including target detection, track initiation, track association, track update, track smoothing, and track termination. The ADS helps to improve the accuracy and reliability of target tracking by using advanced algorithms to filter out noise and other unwanted signals. Once the data has been processed, it is then displayed on an operator interface or computer, providing further information for subsequent actions. This final step allows operators to make informed decisions based on the processed radar data.

3.3 Radar Geometry

A radar system serves a diverse range of purposes, with its most frequently employed applications encompassing the essential functions of detection, tracking, and imaging. Nevertheless, the primary objective of a radar system will always be to measure the *range*, or

distance, of a target. This is accomplished by determining the time it takes for a radar signal to propagate from the source, reflect off the target, and return to the receiver. If the target is not directly in line with the radar, the angle at which the radar antenna is pointed can be used to determine the target's range.

It is possible to derive the range estimation by utilizing the distance formula. The radar transmits a pulse at some time t_1 and the reflected echoes arrive back to the receiver at t_2. Considering that the signal propagates in the medium at a constant speed c, where c is the speed of light, then the range estimation can be expressed as:

$$R = \frac{c\Delta_t}{2}, \tag{3.1}$$

where Δ_t is the time difference t_1 - t_2 and represents the round-trip time between the radar and the object, while the factor $\frac{1}{2}$ stems from the fact that only half of the round-trip time is required to calculate the range R. A monostatic radar employs a spherical coordinate system to measure the position P of a target, with its origin situated at the phase center of the radar antenna. This coordinate system, as illustrated in Figure 3.3, is characterized by the antenna's boresight direction, which is aligned along the positive x-axis. The azimuth angle θ and the

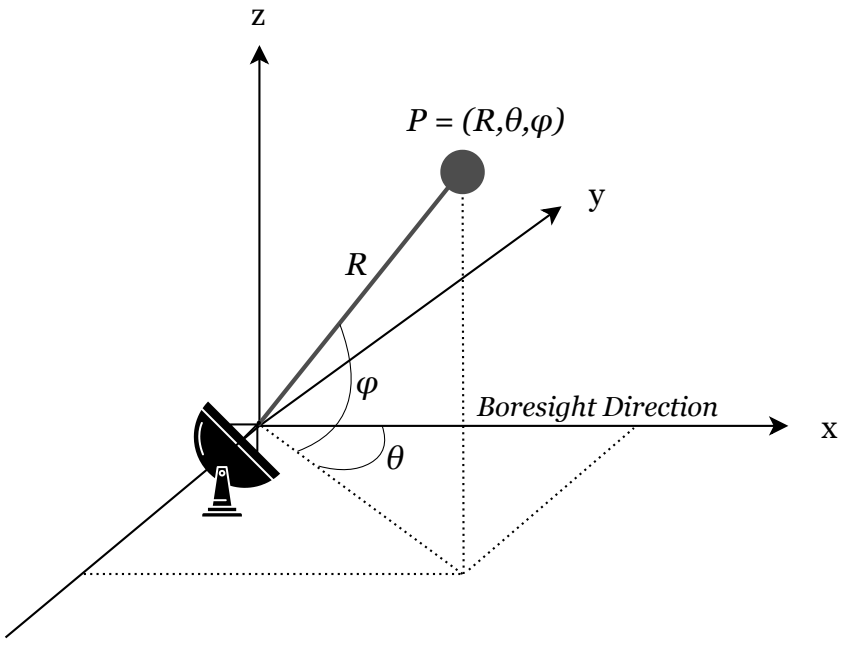

Figure 3.3: The spherical coordinate system used for radar measurements, with the target located at point P [12].

elevation angle φ are used to obtain the direction of the target, relative to the radar system.

These angles can be determined from the antenna's orientation, as the target must typically be located in the antenna's main beam to be detected.

On the contrary, the range R of a target can be directly derived from the elapsed time between transmission and detection, as described in Eq. (3.1), which provides information on the absolute distance between the antenna and the target, without disclosing any further details. Therefore, targets situated at the same distance from the antenna may not occupy identical positions. This situation is accurately presented in Figure 3.4, where targets 1 and 2 are positioned in a circular trajectory from the antenna, drawn as a dashed line. The radar calculates the same range measurements for these targets, but in reality they are not co-located. Consequently, determining the position of a target requires not only its range from the antenna, but also its elevation and azimuth angles.

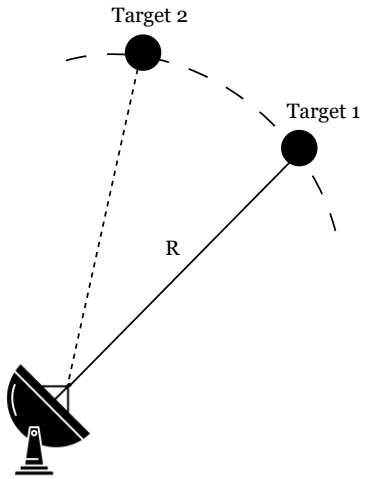

Figure 3.4: Targets located in a circular trajectory have the same absolute range from the antenna but do not occupy the same position [15].

3.4 Range Equation

As previously stated in Section 3.2, it is understood that a monostatic pulse radar operates by transmitting a pulse of RF energy from an antenna and then the receiver listens for echo signals. These returned signals represent reflections from a distant object or target. The strength of the returned signals is dependent upon various factors such as the transmitted power, the distance to the reflecting target, and the electrical size or reflectivity of the target.

To further elucidate this concept, it is important to note the existence of the *radar range equation*, a deterministic model [8, 15, 16] that serves as a valuable tool for both system design and analysis. By establishing a relationship between the received echo power (P_r) and the transmitted power (P_t), this equation correlates the range of a radar and the characteristics associated with the radar components, target, and environment. Its utility extends beyond the determination of the maximum range at which a given radar can detect a target, as it also provides insights into the factors that impact the performance of the radar.

In the event that the transmitted power P_t is radiated by an *isotropic antenna*, i.e. an antenna that distributes power equally in all directions, the *power density* P_d, or the amount of power per unit area carried by the radiation, at a distance R from the radar, is derived by:

$$P_d = \frac{P_t}{4\pi R^2}, \tag{3.2}$$

where P_d is measured in $\frac{Watt}{m^2}$. Radar systems however, often emit electromagnetic radiation in particular directions, which necessitates the use of *directive antennas* with narrow beamwidths, to effectively concentrate the radiated power in the intended direction. The measure of the increased power density radiated in a specific direction, relative to the power density that would arise in that direction from a lossless isotropic antenna, is known as *gain*. When the power density is maximized, then this value is referred to as *G*, and Eq. (3.2) can be rewritten as follows:

$$P_d = \frac{P_t G}{4\pi R^2}. \tag{3.3}$$

When electromagnetic radiation is transmitted, a fraction of the energy interacts with a target, which in return reflects it back in a variety of directions. The power density of the radiated energy, that is redirected towards the radar's direction, is the primary focus of interest. This directional power density can be mathematically expressed as:

$$P_d = \frac{P_t G}{4\pi R^2} \cdot \frac{\sigma}{4\pi R^2}, \tag{3.4}$$

where σ is the *radar cross section* (RCS) of a target. RCS is the equivalent area seen by a radar [17], and has units of area. However, RCS is not directly associated with the target's physical size, but is dependent on the target's shape.

The antenna on the other hand captures a portion of the received electromagnetic energy. The amount of power that is received at the radar is influenced by two main factors: the incident power density P_d, that is derived by Eq. (3.4), and the *effective area* A_e of the receiving

antenna, which is a measure of the antenna's ability to capture the incident energy. The effective area is reliant on the physical area A of the antenna as $A_{\mathrm{e}} = A\rho_{\alpha}$, where ρ_{α} is the *antenna aperture efficiency*, i.e., a dimensionless parameter between 0 and 1 that indicates the degree to which the antenna utilizes all the radio wave power that intersects its physical aperture [18]. Thus, the received power $\mathrm{P_r}$ is expressed as:

$$P_{\mathrm{r}} = \frac{P_{\mathrm{t}} G A_{\mathrm{e}} \sigma}{(4\pi)^2 R^4}. \tag{3.5}$$

The transmitting gain G can be also expressed as:

$$G = \frac{4\pi A_{\mathrm{e}}}{\lambda^2} \Leftrightarrow A_{\mathrm{e}} = \frac{G\lambda^2}{4\pi}, \tag{3.6}$$

where λ is the wavelength of the radiated wave. Substituting Eq (3.5) with Eq. (3.6) will result in:

$$P_{\mathrm{r}} = \frac{P_{\mathrm{t}} G^2 \lambda^2 \sigma}{(4\pi)^3 R^4}. \tag{3.7}$$

Thus far, the influence of *atmospheric attenuation*, denoted by the factor $\mathrm{L_{at}}$, has not been accounted for. The presence of gases in the atmosphere can lead to the attenuation of a signal, by absorbing energy from the propagating wave. By incorporating the attenuation factor into Eq. (3.7), the resulting expression will have a more comprehensive form:

$$P_{\mathrm{r}} = \frac{P_{\mathrm{t}} G^2 \lambda^2 \sigma}{(4\pi)^3 L_{\mathrm{at}} R^4}. \tag{3.8}$$

By solving for the variable R in Eq. (3.8), it is possible to obtain the ultimate expression for the radar range equation, as shown in Eq (3.9). If the minimum ratio between the transmitted and received power is known, it becomes feasible to derive the maximum detectable range of a target.

$$R = \left(\frac{G^2 \lambda^2 \sigma}{(4\pi)^3 L_{\mathrm{at}}} \cdot \frac{P_{\mathrm{t}}}{P_{\mathrm{r}}}\right)^{\frac{1}{4}}. \tag{3.9}$$

These simplified versions of the range equation may not provide an accurate depiction of the actual performance of radar systems, as several additional parameters must be taken into account. Despite this limitation, these simplified equations are deemed adequate for the scope of this thesis.

3.5 Waveform Analysis

In the context of radar systems, the choice of a radar waveform determines several fundamental radar metrics, including the signal-to-noise ratio (SNR), the range/Doppler resolution

and the ambiguities in range/Doppler. The selection process takes into consideration multiple other factors, including the cost and complexity associated with implementing a particular hardware and software solution, as well as the desired radar performance. Therefore, the classification of radar systems based on waveform types leads to two distinct categories: Pulsed radar systems and Continuous Wave (CW) radar systems.

3.5.1 Pulsed Waveforms

Pulsed radar systems [12, 19] utilize a single pulse or a series of modulated pulsed waveforms with varying characteristics to achieve accurate measurements of target properties. The transmitted signals, in conventional pulsed radars, are narrowband and passband, and they are mathematically represented as:

$$x(t) = a(t)\cos\left(2\pi f_c t + \theta(t)\right). \tag{3.10}$$

Here, a(t) represents the constant amplitude pulse envelope, f_c denotes the RF carrier frequency, while θ(t) represents either a constant or a phase modulation of the pulse. In general, it is assumed that a(t) is an ideal, square pulse envelope of amplitude A and τ seconds duration.

As previously discussed in Section 3.3, a pulsed radar can measure the range of a target by calculating the round-trip-time Δ_t of the emitted radiation between the two objects. A train of short-time pulses, each of width τ, is transmitted in time, with each modulated pulse sent after an interval of PRI seconds (PRI standing for Pulse Repetition Interval). The transmission of these pulses is illustrated in Figure 3.5.

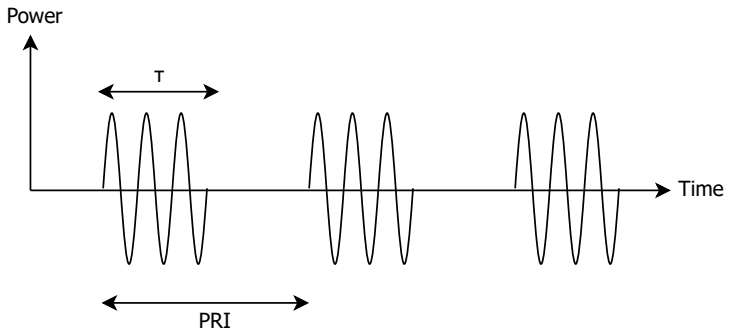

Figure 3.5: Transmission of passband modulated pulsed waveforms. Each pulse is of width τ and is repeatedly emitted after an interval of PRI seconds.

In order to prevent potential damage to the sensitive receiver circuits, due to the high-power transmitted signal leakage, it is essential to isolate the radar receiver from the antenna during pulse transmission. Therefore, for the first τ seconds after pulse transmission begins, the duplexer turns the receiver off, resulting in a *minimum range* of $R_{\text{min}} = \frac{c\tau}{2}$ meters, from which a complete echo can be received.

This becomes more evident when analyzing the baseband signals. Figure 3.6 demonstrates the transmission of baseband pulses, of width τ and amplitude A. During the time period PRI - τ, the antenna is in receive mode, allowing it to receive signal echoes from the target. However, if the time taken by the radar pulse to complete a round trip is longer than the PRI, then the radar may receive the echo of a prior pulse after the next pulse is transmitted, causing ambiguity in the measured range. To avoid this, the PRI must be greater than Δ_t, giving rise to the concept of *maximum unambiguous ranging*. Maximum unambiguous range refers to the maximum distance R_{ua} that a radar can measure a target without any ambiguity in the returned signal, and it can be calculated using the formula:

$$R_{ua} = \frac{c}{2} t_{ua} \tag{3.11}$$

where c is the speed of light and t_{ua}, is the time difference PRI - τ in which radar signals can be received without uncertainties.

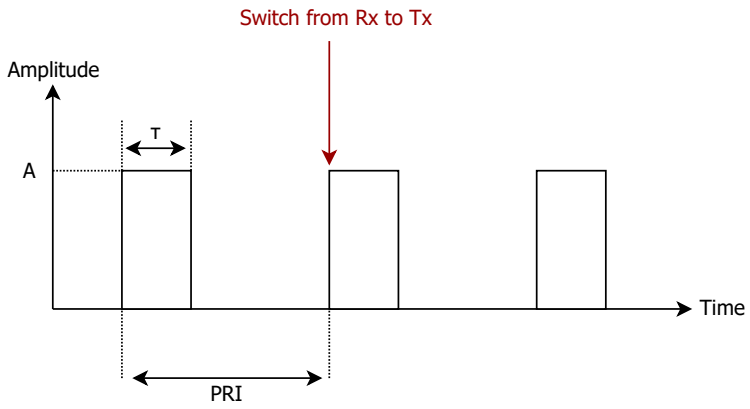

Figure 3.6: Baseband rectangular pulses of width τ and amplitude A, each transmitted every PRI seconds. After the end of the first PRI interval, the antenna is switching to transmitting mode.

In general, the signal at the receiver output will be a combination of delayed echoes of $x(t)$ from targets, clutter and noise. For this reason, they are also narrowband signals, despite

the fact that their amplitude and phase modulation will typically be altered due to propagation loss and Doppler shifts. Thus, the received signal, resulting from a single pulse echoing from a target at range R_0:

$$y(t) = k \cdot a\,(t - t_0)\, e^{j[2\pi f_c(t-t_0)+\theta(t-t_0)+\phi(t)]} + n(t), \tag{3.12}$$

where n(t) is an additive random noise, k is the echo amplitude factor that describes the attenuated signal due to propagation losses and target reflectivity, and $\phi(t)$ is the echo phase modulation due to target interaction.

In the case of multiple targets being present in the vicinity of a radar, the received signal may include echoes from all the of them. However, if these targets are in close proximity between them, then these echoes may overlap, making it difficult to decipher the received information. Therefore, to overcome this challenge, radars introduce an important metric, known as *range resolution*, which is one of the most crucial parameters of a radar system. Range resolution, denoted as Δ_R, refers to a radar system's ability to distinguish between two or more targets, situated in the same angular direction but at different ranges. The efficacy of range resolution relies on various factors such as the width of the transmitted pulse, size and nature of targets, and the proficiency of the receiver and indicator. Nevertheless, the pulse width is the primary determinant of range resolution.

Figure 3.7(a) depicts a simple two-stationary-target system, wherein a single pulse of width τ, as the one in Figure 3.7(b), initiates transmission at t = 0. The first target is located at a distance of R_0 from the radar, while the second target is located at $R_0 + \Delta_R$. The pulse propagates through the medium at the speed of light and reaches targets 1 and 2, which reflect back the radiation in the form of shifted, lower energy pulses, as shown in 3.7(c). Notably, the echoes from the two targets are in close proximity without overlapping. Therefore, the minimum distance between the targets that prevents overlapping is mathematically expressed as:

$$\Delta_R = \frac{c\tau}{2}. \tag{3.13}$$

Eq. (3.13) emphasizes that for a radar to distinguish between two targets, their distance should be greater than Δ_R. Figure 3.7(d) confirms this assertion, as the second echo from target 2 overlaps with the first echo, which had not yet been fully received, proving that the stationary targets where too close to be distinguished. Reducing the pulse width can prevent overlapping echoes, but it also decreases range resolution, as per the inverse relationship

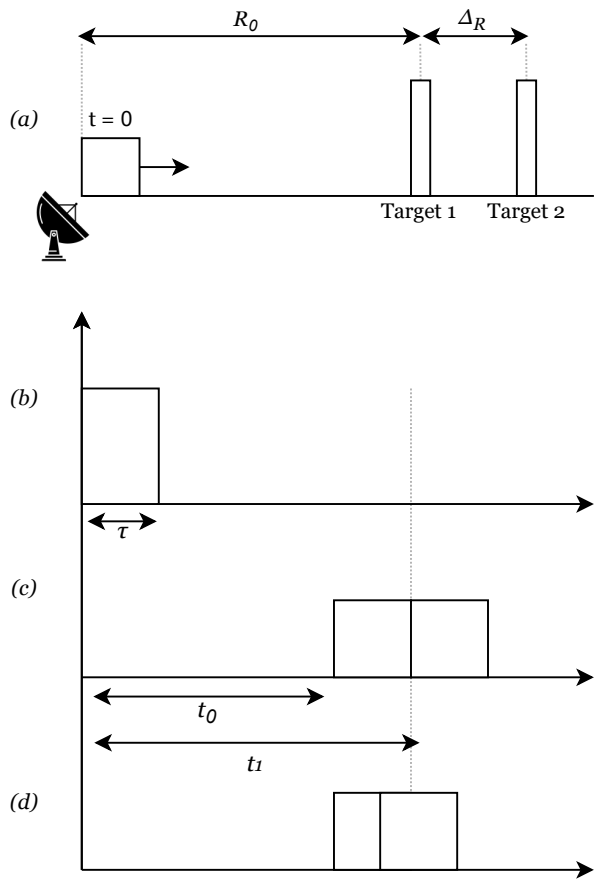

Figure 3.7: (a) A simple two-target model. Targets 1 and 2 are located at a distance of R_0 and $R_0 + \Delta_R$ correspondingly, and reflect the transmitted pulse; (b) the transmission of the single pulse at t = 0; (c) the borderline case of non overlapping echoes; (d) overlapping.

between pulse width and spectral bandwidth $BW = \frac{2}{\tau}$. Narrower pulses have wider bandwidths, which can increase the complexity of radar systems and necessitate advanced signal processing methods. Furthermore, as per the relationship between the pulse's energy and its width $E = A^2\tau$, by reducing the pulse's width, the energy transmitted per pulse will decrease, potentially reducing the radar's detection range for distant targets. Therefore, the balance between range and resolution must be carefully weighed when designing a radar system.

3.5.2 LFM Waveforms

On the contrary, when it is desired to increase the transmitted energy for a given power level, then the rectangular pulse requires an increase in its width. However, elongating the pulse results in a decrease in its instantaneous bandwidth, which causes a degradation in the range resolution. Therefore, sensitivity and range resolution seem to contradict each other.

Fortunately, the technique of *pulse compression* [19, 20] provides a solution to this problem, by decoupling the pulse duration from its energy. This is achieved by creating different durations for the transmitted pulse and processed echo, which can be done by designing a frequency modulated pulsed waveform instead of using a constant-frequency pulsed one. One popular option is the *linear frequency modulated* (LFM or ”chirp”) waveform, an example of it illustrated in Figure 3.8.

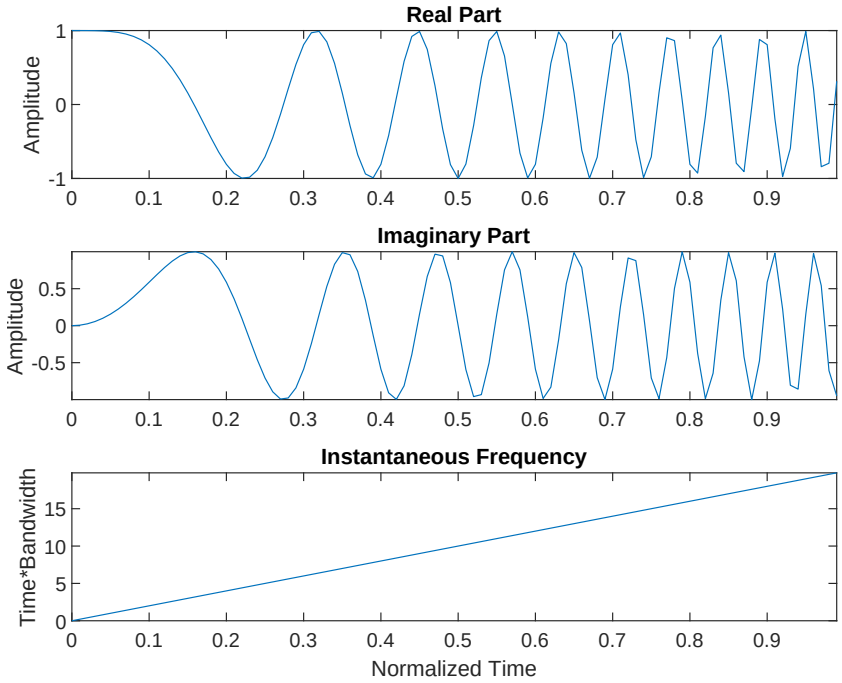

Figure 3.8: The real and imaginary part of an LFM waveform, along with its instantaneous frequency. Here, the frequency increases with time, with a positive slope β and at a constant rate.

An LFM pulse can be mathematically defined as:

$$x(t) = \cos\left(\frac{\pi\beta}{\tau}t^2\right), \quad 0 \leq t \leq \tau, \tag{3.14}$$

where β is the sweep bandwidth. The complex equivalent can be expressed as:

$$x(t) = e^{j\pi\frac{\beta}{\tau}t^2} = e^{j\theta(t)}, \quad 0 \leq t \leq \tau. \tag{3.15}$$

The instantaneous frequency (in Hz) of this waveform is the time derivative of the phase function θ(t):

$$F_i(t) = \frac{1}{2\pi} \cdot \frac{d\theta(t)}{dt} = \frac{\beta}{\tau}t. \tag{3.16}$$

During the pulse duration, the instantaneous frequency $F_i(t)$ sweeps linearly across over the desired bandwidth β, as Figure 3.8 presents. This frequency sweep can either increase or

decrease, but the rate of frequency change remains constant. The slope of $F_i(t)$ is simply β; when β is positive, the pulse is an upchirp, but if β is negative, then it is a downchirp.

3.5.3 FMCW Waveforms

The case study of this thesis employs a waveform known as a *Frequency Modulated Continuous Waveform* (FMCW), which is based on the fundamental principles of LFM waveforms. The key difference between these two waveform types is that when using an FMCW, the frequency of the transmitted signal continuously varies by means of a modulating signal, at a known rate and over a fixed time period, and returns to its starting point at the end of each sweep. On the contrary, in LFM waveforms, the frequency linearly increases or decreases over time, depending on the sign of β. Various frequency modulation techniques can be employed, with *sawtooth* and *triangular* modulations being the most commonly used methods for altering the frequency pattern of the emitted radio wave, as reported in the literature [21].

Figure 3.9 displays a snapshot of an FMCW waveform for 2 sweeps. The system emits a continuous wave at a specific frequency, and subsequently modulates it over time T, providing the signal with a "time stamp". Then, the modulated waveform propagates to the target and a portion of it is reflected back to the radar. The FMCW approach produces a returned signal

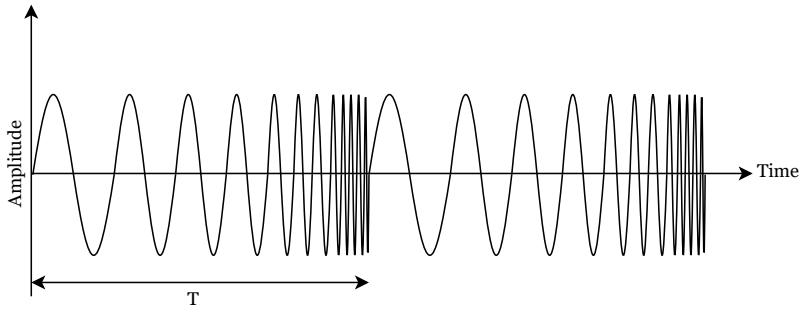

Figure 3.9: The up-chirp waves, using sawtooth modulation. The frequency of the continuous waveform increases with time during the sweep.

that resembles the initial signal [22]; however, as illustrated in Figure 3.10, the frequency of the received signal deviates from that of the transmitted signal by an amount of Δf, which results from the time delay between transmission and reception, and it is also shifted by Δ_t, due to the two way propagation. The mixer stage in the receiver circuit calculates this frequency difference Δf, or most commonly known *beat frequency* f_b, by mixing the received signal frequency with the transmitted frequency. The beat frequency is directly proportional

to the range distance R_0 and can be utilized to determine the distance using the following equation:

$$R_0 = \frac{cf_b\tau}{2\beta}. \tag{3.17}$$

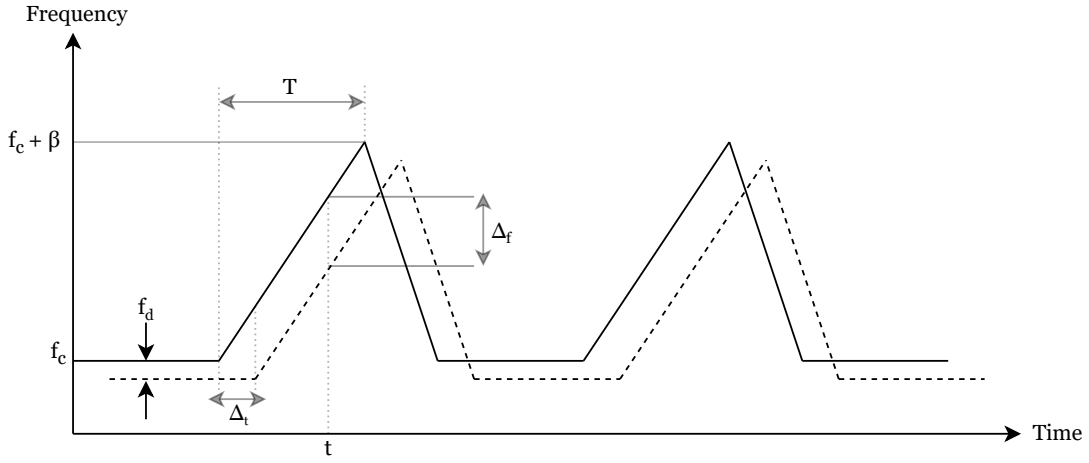

Figure 3.10: The instantaneous frequencies of an FMCW signal and its echoed response, utilizing sawtooth modulation. The dashed lines indicate the received signal, which is shifted in both the frequency and time domain. A moving target is considered, resulting in the appearance of the doppler frequency f_d, that will be utilized to determine its velocity [22].

3.6 Doppler Analysis

The Doppler effect gives rise to the concept of Doppler frequency f_d, which is a result of the frequency alterations that occur when an object moves relative to the radar system. This means that if the targeted object has a radial speed u, with respect to the receiving antenna, and the signal is observed over several periods, then this additional Doppler frequency shift f_d can be detected. In monostatic radars, the connection between the velocity of a moving target and its resulting frequency shift, can be extracted by the formula:

$$f_d = \frac{2f_c}{c}\, v, \tag{3.18}$$

where v is the velocity of the moving target and f_c is the carrier frequency of the transmitted signal. If the target is moving with some velocity v_0 at an angle θ, with respect to the line connecting the radar, then the radial velocity is determined by $v = vocos(\theta)$.

When the returned echoes contain signals from both stationary (clutter) and moving targets, the received signal is a superposition of these signals. If the target is moving towards the radar, the frequency of the entire echo signal increases at $f_c + f_d$, while if the object is moving away from the radar, the frequency decreases at $f_c - f_d$.

It is noteworthy to mention that when various parts of a target vibrate or rotate, they produce an additional frequency modulation, alongside the Doppler shift caused by the target's motion. This phenomenon is commonly referred to as the "micro-Doppler effect", and a substantial portion of this study is dedicated to its analysis and exploration. For instance, the rotation of a vehicle's wheels or the blades of a helicopter, both generate unique radar micro-Doppler signatures. Similarly, in humans, the varying motion of the torso, arms, legs, hands, and feet produces a distinct micro-Doppler signature that can be visually distinguished from other targets.

Mathematically speaking, the micro-Doppler signatures are obtained through a Time - Frequency (TF) transform of the complex I/Q radar data, which are represented as:

$$I = A\cos\left(2\pi ft + \phi_0\right), \quad Q = A\sin\left(2\pi ft + \phi_0\right) \tag{3.19}$$

This transformation allows the observation on how the received Doppler frequencies change over time. There are two main categories of TF analysis methods: *linear transforms* and *quadratic time-frequency distributions* (QTFDs). In this thesis, the focus is on studying linear transforms, particularly the Short-Time Fourier Transform (STFT).

The most commonly used TF transform is the *spectrogram*, denoted as S(t,ω), which is the squared modulus of the STFT. It can be expressed in terms of the employed window function, w(t), as:

$$S(t,\omega) = \left| \int_{-\infty}^{\infty} w(t-u)x(u)du \right|^2 \tag{3.20}$$

While benefiting from linearity, STFTs face a trade-off between TF resolution and fixed window length. More detailed information about these transforms can be found in extensive research, available in the literature [23, 24].

3.7 Signal Processing

The domain of radar signal processing involves the digital processing of receiving signals, with the goal of extracting the requisite information, while concurrently suppressing

the unwanted echoes arising from various sources, due to clutter, atmospheric conditions, RF interference, noise sources, and deliberately produced jamming signals. In recent years, the need for advanced signal processing techniques has grown exponentially, due to the increasing demands of modern radar systems to detect targets and extract critical parameters from the received waveforms with high accuracy, such as their position, velocity, shape, and Doppler signatures. In order to get information from the received signal, the signal and radar processors use different methods and techniques, including Matched Filters (MF) [25], Moving Target Indicators (MTI) [26], Doppler Filtering [27], and Space-Time Adaptive Processing (STAP) [28].

3.7.1 Matched Filters

As any other signal transmitted over the air, the chirp signal, i.e., the signal in which its frequency increases or decreases in time, encounters noise during its propagation. In the simple case of the collected signal being an exact replica of the transmitted signal, reflected by a stationary target, but delayed per t_0, it can be expressed as:

$$y_t = x(t - t_0) + n(t), \tag{3.21}$$

where n(t) is white noise. The presence of noise and other attenuating factors can make the detection process challenging, and improving the signal-to-noise ratio (SNR) can significantly enhance the performance of the system. To maximize the SNR at the receiving end, a Matched Filter (MF) can be utilized. To determine the optimal receiver frequency response H(Ω) that would optimize the SNR, it is necessary to consider the received signal's power. The received signal's spectrum can be expressed as $Y(\Omega) = H(\Omega)X(\Omega)$, where $X(\Omega)$ denotes the transmitted waveform's spectrum. The power of the received signal at an arbitrary time t_m can be computed by implementing the inverse Fourier transform of $Y(\Omega)$ as:

$$|y\left(t_m\right)|^2 = \left|\frac{1}{2\pi}\int_{-\infty}^{\infty} X(\Omega)H(\Omega)e^{j\Omega t_m}d\Omega\right|^2. \tag{3.22}$$

Considering the case where the interference is white noise, with power spectral density ${\sigma_w}^2$. The noise power spectral density at the output of the receiver will be ${\sigma_w}^2 H(\Omega)$. Thus, the total output noise power is given by the formula:

$$n_p = \frac{\sigma_w^2}{2\pi}\int_{-\infty}^{\infty} |H(\Omega)|^2 d\Omega. \tag{3.23}$$

To determine the optimal receiver frequency response H(Ω) that maximizes the SNR, Eq. (3.22) and (3.23) are first divided. The choice of H(Ω) that will maximize the division's result can be determined via the Schwarz inequality [12], resulting in:

$$\begin{aligned} H(\Omega) &= \alpha X^*(\Omega) e^{-j\Omega t_m} \text{ or} \\ h(t) &= \alpha x^* \left(t_m - t\right). \end{aligned} \tag{3.24}$$

Here, α is the gain constant, often set equal to unity, and $x^*(t)$ is the complex conjugate of the transmitted signal.

The resulting response $H(\Omega)$, derived from Eq. (3.24) is known as a *matched filter*, as it is precisely "matched" to the transmitted waveform, and they are required to be a matched set in order to maximize the output SNR. By time-reversing the H(Ω) spectrum, the impulse response $h(t)$ of the matched filter is obtained. If the radar system changes the type of the transmitted waveform, then the receiver filter response must also be adjusted to maintain a matched condition. Figure 3.11 illustrates a general block scheme of an MF.

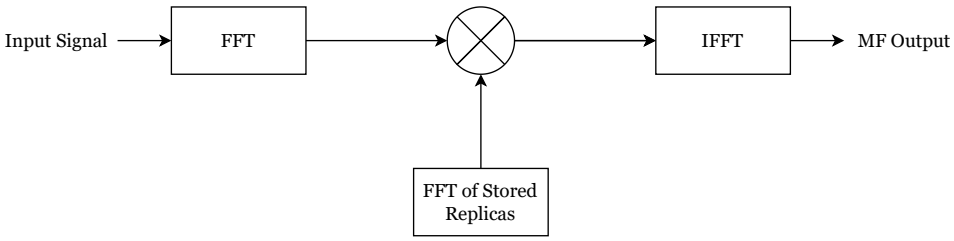

Figure 3.11: Block diagram of a Matched Filter.

Supposing that the input signal in Figure 3.11 is the echo from a stationary target at an unknown range R_0. The delay can be then be derived by the relationship $t_0 = \frac{2R_0}{c}$. On the other hand, the output of the MF can be mathematically expressed as the convolution of the received signal, in the time domain, with the MF's output response:

$$y(t) = \int_{-\infty}^{\infty} x\left(s - t_0\right) \alpha x^*(s + \tau - t) ds. \tag{3.25}$$

As presented in Figure 3.12, the output response $y(t)$ will appear as a triangle, with its peak occurring at $t_{peak} = t_0 + \tau$. This t_{peak} corresponds to the actual, two way delay to the target t_0, plus the delay of the MF, which is equal to the waveform's width τ. The target range can be easily determined as $R_0 = \frac{c\ (tpeak - \tau)}{2}$.

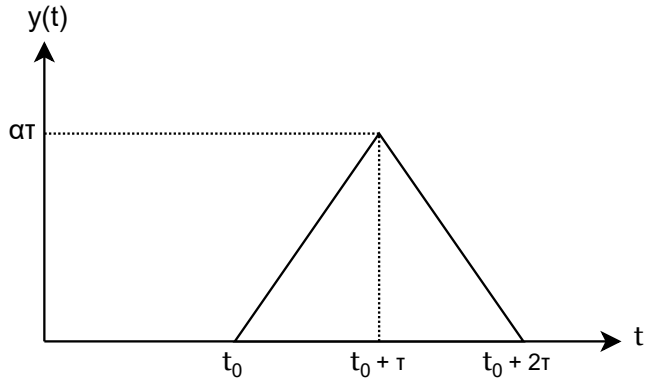

Figure 3.12: Output response of the MF for a stationary target at range $R_0 = \frac{ct_0}{2}$.

3.7.2 Detection Theory

Although the approach so far may appear redundant in straightforward cases, such as those lacking noise, the presence of noise and clutter in real-world scenarios renders the issue of *detection* [29], which is considerably more complex and extensively studied. In a nutshell, radar systems encounter the challenge of separating the useful target echoes from the interference background that hinders the target detection. Therefore, the primary objective of a radar processor is to determine whether the collected echoes contain useful signal components that convey information about a potential target, or if they are simply comprised of noise/clutter. This issue can be framed in the context of a binary hypothesis test, where:

1. H_0: Null Hypothesis; there are only contributions from interference.

2. H_0: Alternative Hypothesis; there are contributions from both interference and echoes from a target.

In Figure 3.13, the output response of a received pulse contains both useful data and white noise. In the presence of noise, distinguishing between these components can be quite difficult. To mitigate this problem, an MF can be employed, which effectively reduces noise and clutter, thus subsequently enhancing the SNR of the overall signal. The MF response exhibits a prominent peak, signifying the existence of a target and, thus, enabling the accurate estimation of crucial target parameters such as its range.

On closer inspection of Figure 3.14, it is evident that the received pulse, depicted in the upper plot, is simulated with a higher level of noise. Despite the use of an MF, the presence of a target in the radar's vicinity still remains uncertain. Even though the received signal is

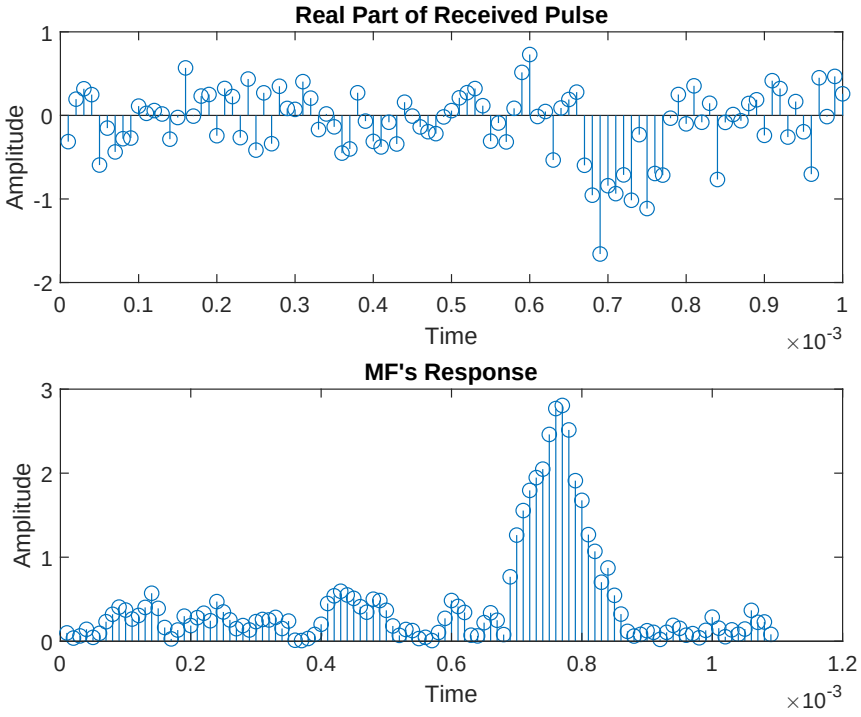

Figure 3.13: Output response of a noisy pulse at the receiver's end (upper plot) and at the output of a Matched Filter (lower plot). Despite the knowledge that a target is present in the radar's vicinity, extracting valuable target information from interference in noisy environments is a challenging task that necessitates the use of various signal processing techniques.

comprised of multiple peaks, not all of them are relevant for detecting the presence of a target. As previously established, a peak must exceed a certain *threshold level* to be considered indicative of a target. The hypothesis test described earlier is utilized to determine whether a target is present or not. Each measurement, collected by the radar system, is subjected to this test, and the hypothesis that best fits the data is chosen. The threshold level can be computed using various techniques that are found in the literature, such as the Neyman-Pearson (NP) detection rule [30], Likelihood Ratio Test (LRT), and the Log-Likelihood Ratio Test (LLRT) [29].

On a final note, the clutter and/or hostile noise jamming in radar systems can often surpass the receiver's internal noise, leading to an increase in the detection threshold and subsequent false alarms. False alarms on radars occur when the radar system detects a signal that is not actually a target of interest. To combat this issue, the popular technique of *Constant False Alarm Rate* (CFAR) [31] is utilized to automatically adjust the threshold level and prevent the system from becoming overloaded with irrelevant information, ultimately reducing the incidence of false alarms. However, while CFAR is effective at mitigating false alarms, it can

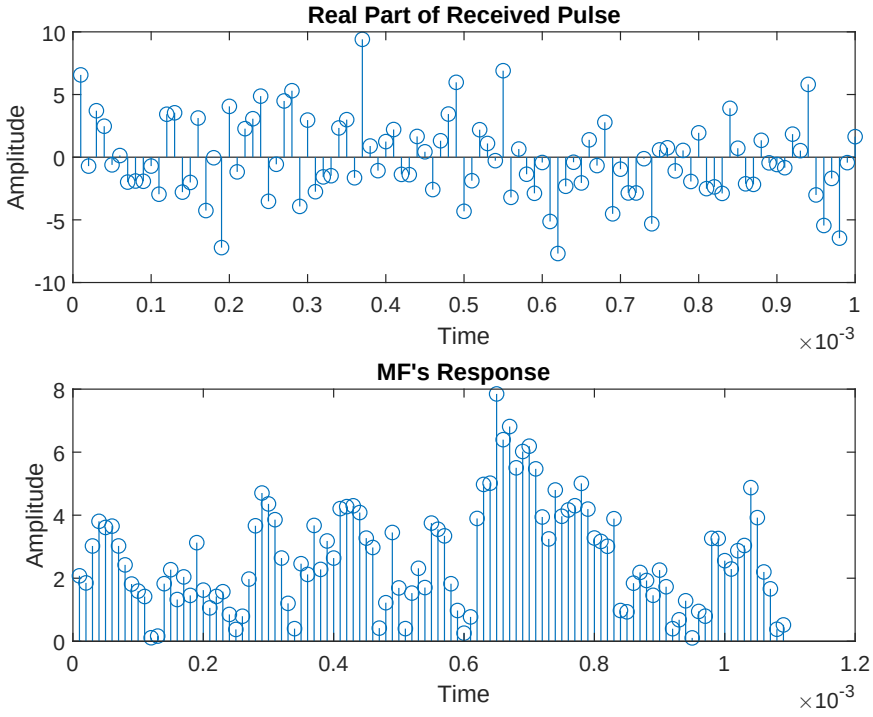

Figure 3.14: Output response of the same pulse as in Figure 3.13, but with increased noise levels, highlighting the difficulty in differentiating the target from interference, even with the use of an MF.

also decrease the probability of detecting actual targets.

3.8 Phased Array Systems

Radar antennas are a fundamental part of any radar system, as they are responsible for the sensitivity and angular resolution of the radar. Their primary function is to convert electrical signals into electromagnetic waves and vice versa.

A plethora of antenna types are employed in radar systems, each with distinct advantages and limitations. While the theoretical isotropic antenna [8, 14] serves as a reference for measuring the performance of practical antennas, it does not exist in reality. In practice, nearly all radar antennas are directive and have some form of beam-steering mechanism, allowing them to emit narrow beams of radiation in specific directions. This feature is particularly important, as it enables accurate angular measurements and the ability to resolve closely spaced targets, which would be impossible with a non-directive antenna.

A fascinating aspect of antenna systems is the ability to alter the radiation pattern by arranging the antennas in specific configurations, without physically moving them. This leads

to improved gain, directivity, and overall performance in a desired direction. Such configurations are known as *phased arrays*, which find extensive use in modern radar systems, due to their numerous advantages. The fundamental principle of a phased array system is based on the superposition of two or more radiated signals. When these signals are in-phase, they constructively interfere, leading to an additive amplitude signal. Conversely, when the signals are out-of-phase or counter phase, they destructively interfere and cancel each other out. This phase-dependent property allows the radiation pattern to be steered electronically by adjusting the relative phases of the signals across the individual antennas in the array. Consequently, the direction of the beam can be adjusted without the need for mechanical movement of the antenna system, enabling the phased array to track moving targets or respond to changing environmental conditions very rapidly [32].

This property of phased arrays is accurately depicted in Figure 3.15. The upper plot illustrates the radiation pattern of a single, isotropic antenna that uniformly radiates at 0 dB across the range of $-90°$ to $90°$. On the other hand, the lower plot shows how arranging 15 isotropic antennas linearly, separated by $\frac{\lambda}{2}$, creates a narrower beam in the boresight direction, establishing it as the direction of peak gain of the array.

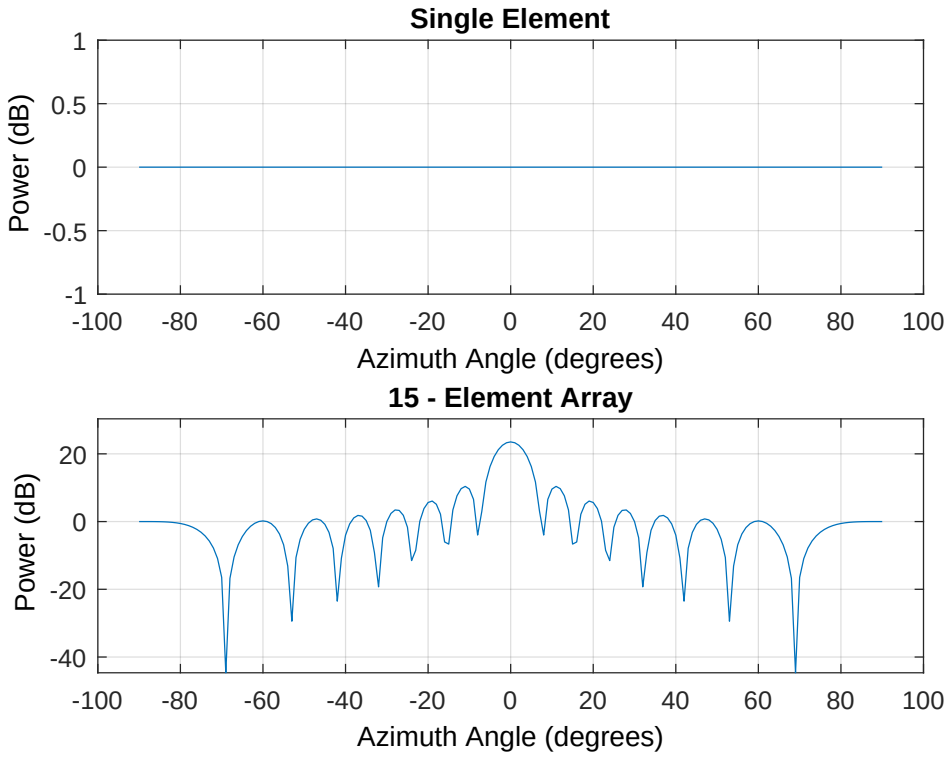

Figure 3.15: Radiation patterns of an isotropic antenna (upper plot) and of a multi-element linear array (lower plot).

Linear arrays, while a well-known type of phased array, are just one among a multitude of available configurations. Scientific literature has extensively documented a diverse array of options that can be employed in place of linear arrays, as evidenced by the extensive coverage in works by Skolnik and Balanis [13, 33].

3.8.1 Uniform Linear Arrays

A part of the case study in this thesis has been conducted by employing a Uniform Linear Array (ULA) [34]. A ULA consists of a series of identical and uniformly spaced apart radiating elements, arranged in a linear topology. The array can be comprised of either isotropic or omnidirectional antenna elements. Isotropic antennas radiate power uniformly in all three dimensions, whereas omnidirectional antennas radiate equal power in all horizontal directions. Throughout the study, it is assumed that isotropic antenna elements are employed, providing a reference point for measuring the performance of real-world antennas.

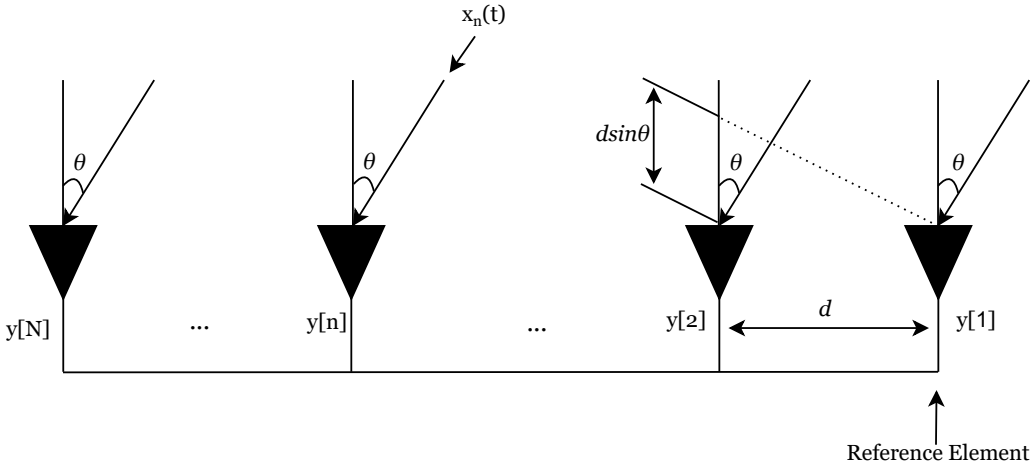

Figure 3.16: System model for DOA estimation using a ULA of N elements [35].

Figure 3.16 illustrates a N-element ULA system, in which, each element is separated by a distance d, restricted to half the wavelength λ of the collected waveform. A source, located in the far field, emits radiation in the form of:

$$x(t) = e^{j2\pi f_c t} \tag{3.26}$$

The elements of the ULA individually collect the incident waveforms that impinge upon them at a specific angle θ, that is also referred to as the *Direction of Arrival* (DOA). The DOA is

typically measured with respect to the boresight direction and is independent of the array's orientation.

In this scenario, the incoming signal is received first by the rightmost element, which is designated as the "reference element". The other elements will receive the signal with a time delay that increases incrementally, due to the geometry of the ULA, and is mathematically expressed as:

$$\tau_n = \frac{(n-1)dsin(\theta)}{c}, \quad 1 \leq n \leq N \tag{3.27}$$

Eq. (3.27) is a function of the distance between the elements, the DOA of the incoming signal, and the propagation speed. Therefore, the output of the n^{th} sensor can be expressed as:

$$y_n(t) = x(t - \tau_n) \Leftrightarrow y_n(t) = x(t)\, e^{2\pi f_c \tau_n}, \tag{3.28}$$

with n ranging from 1 to N. According to Eq. (3.28), it is worth emphasizing that the output of each sensor is dependent on this delay, which is directly related to the phase difference between the signals. Therefore, by carefully examining Eq. (3.27) and (3.28), it is concluded that the output response of each element is directly related to the time delay at which the waveform arrived, giving rise to the concept of the *Steering Vector*. The steering vector is a mathematical representation of the array's directional sensitivity, formulated as:

$$\mathbf{a}(\theta) = \begin{bmatrix} 1 & e^{j2\pi f_c \frac{dsin(\theta)}{c}} & \cdots & e^{j2\pi(N-1) f_c \frac{dsin(\theta)}{c}} \end{bmatrix}^T, \tag{3.29}$$

where fc is the carrier frequency of the incoming waveform. One practical application of the steering vector is to align the array towards the direction of the incoming signal, allowing amplification or suppression of signals arriving from a particular direction, while attenuating signals from other directions [35]. Figure 3.17 illustrates this function, by presenting the response of a 15-element ULA, with half-wavelength spacing between the elements, at a carrier frequency of 24 GHz. In the lower plot, it is evident how the main lobe has steered towards 30° azimuth, in comparison to the upper plot where the narrow beam points in the broadside direction.

Another technique that can also be used for directional signal transmission or reception is *beamforming*. Beamforming is a powerful technique employed in sensor arrays, such as antennas, microphones, and sonars, to improve the detection or transmission of signals in a specific direction. The technique operates as a spatial filter that combines the outputs of individual sensors in the array, in a manner that results in a desired beam pattern with enhanced directivity, while concurrently tries to mitigate interference located at other directions.

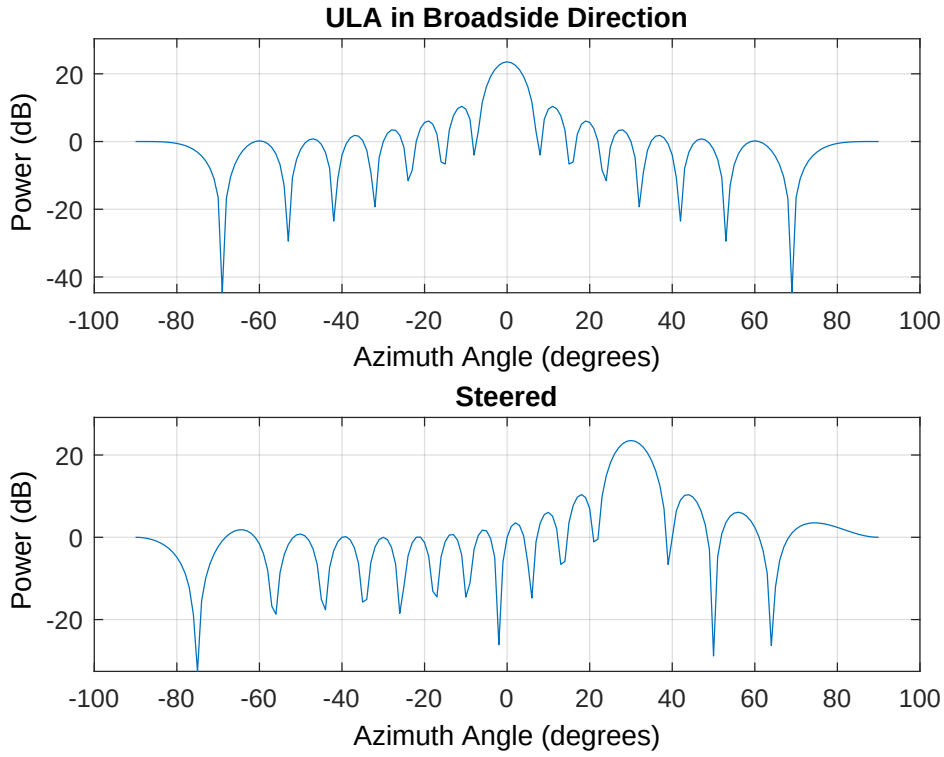

Figure 3.17: Radiation patterns of a 15-Element ULA. In the upper plot, the main lobe points in the broadside direction while in the lower plot, it has steered in the direction of $30°$ azimuth.

Conventional [36] beamformers employ fixed weights for combining the sensor outputs, resulting however in a static beam pattern that cannot adapt to changes in the environment or interference. On the other hand, *adaptive* beamformers, such as the Minimum Variance Distortionless Response (MVDR) beamformer [35], use algorithms that modify the weights based on the incoming signals and the environment, thereby achieving better interference rejection, improved SNR, and better target detection in dynamic environments. However, a critical challenge associated with adaptive beamforming is achieving an optimal balance between reducing antenna sidelobes, and maintaining a narrow mainbeam for high resolution and gain. Sidelobes represent unwanted radiation lobes that emanate from the antenna, in directions other than the main beam. Reducing the sidelobes is crucial for minimizing interference and improving the SNR. Nonetheless, the weights chosen to achieve this reduction lead to a wider mainbeam, resulting in degraded resolution and gain.

To explore these techniques further, the literature provides a wealth of knowledge, including various approaches and advancements in phased arrays and beamforming. Thus, further study and research in these fields can lead to more innovations and advancements in the development of sensor arrays for various applications.

3.9 Radar Sampling

Section 3.3 has provided a thorough explanation of the three-dimensional operation of radar systems. Nowadays, with the advent of digital processing, all of the data processing is performed in a digital format. Consequently, to depict the space-time processing more intuitively, the concept of a *radar data cube* has been introduced.

The radar data cube is a convenient, three-dimensional graphic depiction the space-time processing of sampled radar data. To construct the radar data cube [37], the pre-processing stage converts the RF signals to complex-valued baseband samples, as expressed in Eq. (3.19). This results in the formation of a complex signal $I + iQ$. These samples are arranged in a three-dimensional array of size K×N×L, as illustrated in Figure 3.18. K, defines the length of the *fast-time* dimension, N, the length of the *spatial* dimension, while L, the length of the *slow-time* dimension.

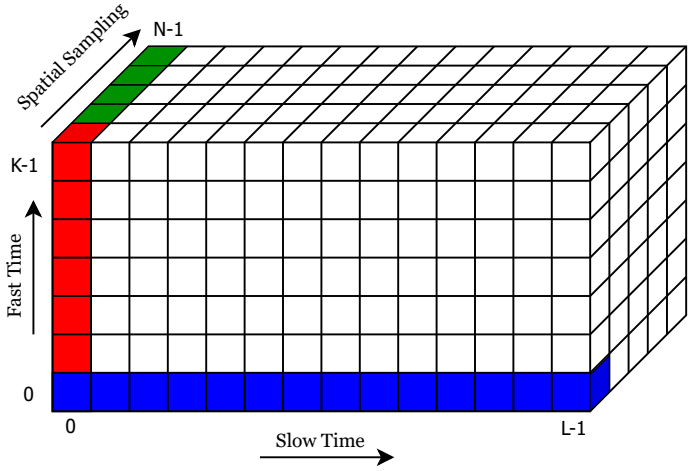

Figure 3.18: An illustration of the radar cube's arrangement [37].

Fast-Time: The fast-time dimension involves the analysis of a K×1 subvectors along the fast-time axis, as illustrated in red in the preceding diagram. Each row in this subvector represents a sequence of complex-valued baseband samples, extracted from a single pulse that was obtained from a specific array element. These samples are acquired at the system's highest sampling rate, denoted as F_s, and consequently, this dimension is designated as fast-time. The sampling interval, T_s, is determined simply as the reciprocal of F_s ($T_s = \frac{1}{F_s}$).

It is noteworthy to mention that the fast-time dimension is also known as the *range dimension*. When fast-time sample intervals are converted to distance, by employing Eq. (3.1),

then the resulting intervals are referred to as *range bins*. The examination of the distribution of radar returns within the range bins is instrumental in constructing range profiles, which in return yield valuable insights into the target's shape and structure.

Slow-Time: Within this dimension, each K×L submatrix in the data cube comprises of K row vectors, with a dimension of 1×L, as illustrated in blue colour in the Figure above. These row vectors represent complex-valued baseband samples, obtained from L different pulses in the same range bin. For each of the N array elements, there is a corresponding K×L matrix. The sampling interval, between L consecutive samples in the slow-time dimension, is commonly referred to as the *pulse repetition interval* (PRI). Typically, the PRI is considerably longer than the fast-time sampling interval, allowing for the acquisition of samples across multiple pulses. Consequently, the samples obtained within this dimension are known as slow-time samples. Through data processing in the slow-time dimension, valuable information regarding the Doppler spectrum at a specific range bin can be derived. By analyzing the variations in the acquired signals over the PRI, the radar system can estimate the frequency content and velocity characteristics of targets within the observed range bin.

Spatial Sampling: The spatial sampling dimension in radar systems plays a vital role in capturing the spatial characteristics of the incident waveform, as phased arrays consist of multiple array elements. Within each K×N submatrix of the radar cube, there are K fast-time samples in each column, obtained from a single pulse at one single array element. In total, the N column vectors, marked in green in Figure 3.18, represent the same pulse sampled across N array elements simultaneously. By examining the data across the array elements, it becomes possible to determine the spatial frequency associated with each received pulse, which is the equivalent of estimating the *angle of arrival* (AOA).

An important technique utilized in this context is *beamforming*. As mentioned earlier, beamforming involves a spatial filtering operation that selectively enhances or suppresses waveform incidents on the array, from specific directions. By intelligently combining the data across the array elements, beamforming allows for improved spatial resolution and the ability to focus the radar system's sensitivity towards desired targets or directions of interest. This technique plays a crucial role in enhancing the radar system's performance in terms of detection and tracking capabilities.

3.9.1 A Processing Example

To further investigate radar processing, an illustrative example of the processing method is being presented in Figures 3.19 and 3.20. In this example, the received FMCW signal that is presented in Figure 3.9 will be sampled for processing.

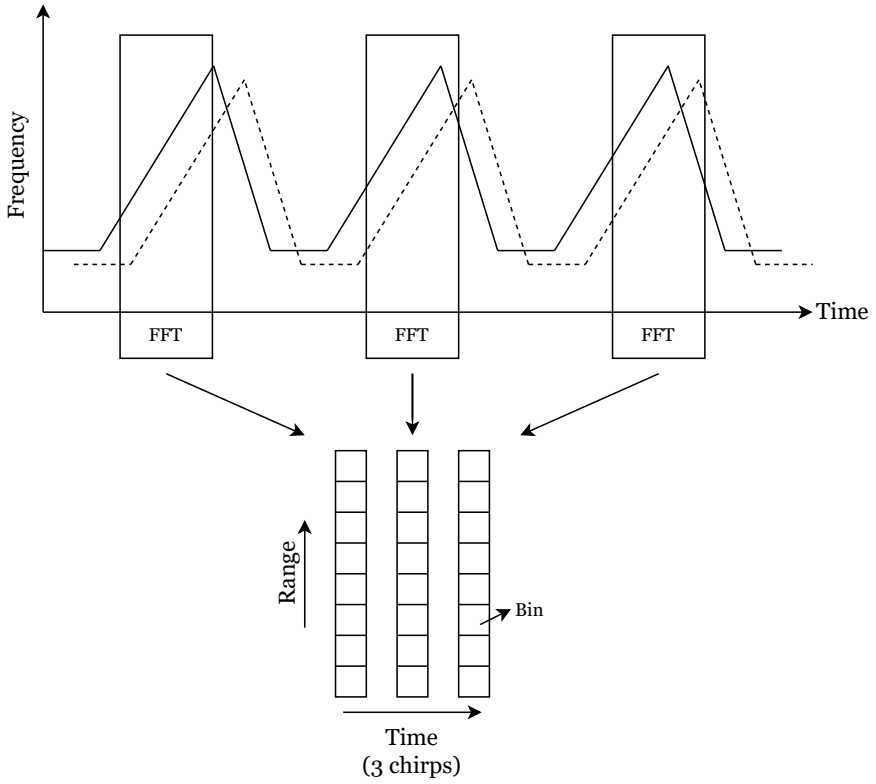

Figure 3.19: Radar Sampling Processing: Application of the FFT algorithm for range estimation [22].

The FMCW signal exhibits an instantaneous frequency $F_i(t)$, as visually represented in Figure 3.10. Figure 3.19 shows that the initial step involves performing a *Fast Fourier Transformation* (FFT) on the received signal. This transformation enables the mapping of each sample to a specific bin. By employing the FFT technique, the FMCW signal undergoes spectral analysis, allowing for the identification and localization of targets based on their range. By repeating this process for each chirp, comprehensive range information across the fast-time dimension can be obtained.

After the acquisition, storage, and processing of all the chirps, a Doppler-FFT analysis can be conducted to extract precise velocity information regarding the target. This evaluation is done once every L chirps in the slow-time. This evaluation occurs periodically, once every L chirps, within the slow-time dimension. Subsequently, the K$\times$L data samples, obtained

across all elements of the array, are merged to form the third dimension of the radar cube. This dimension provides crucial insights into the spatial position of the target, encompassing its spatial distribution within the radar's field of view. By combining the information from multiple array elements, a comprehensive representation of the target's location and movement can be obtained, facilitating accurate target tracking and identification.

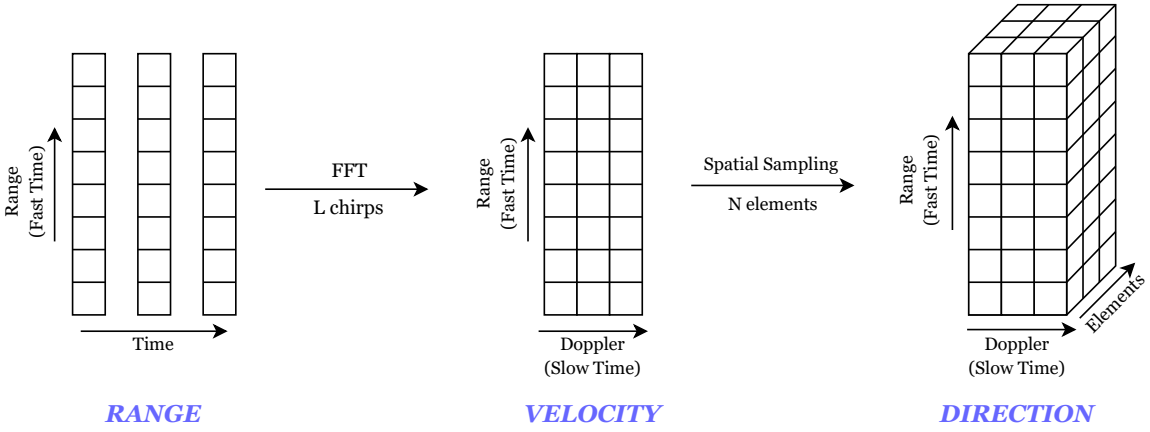

Figure 3.20: Practical illustration of the Radar Data Cube. The far left plot depicts the sampled data, used for range estimation. In the middle, the data combined from multiple chirps are used to calculate the velocity of the target, while in the right plot, data from all of the array elements are combined together to determine the spatial position of the target [22].

In conclusion, this fusion of data across the elements further enhances the three-dimensional characterization of the radar cube, enabling precise analysis and interpretation of the target's spatial attributes.

Chapter 4

Deep Learning for Radars

4.1 Introduction

Deep Learning (DL) [23] is an exciting and rapidly advancing branch of *Machine Learning* (ML), that has made significant progress in addressing complex challenges in computer vision and natural language processing. It has outperformed traditional methodologies that were previously regarded as cutting-edge. The key to this success lies in the utilization of deep neural networks (DNNs), which distinguish themselves from conventional approaches by focusing more on automatic feature learning, rather than manual feature engineering and model training. By capitalizing on extensive datasets, DNNs have demonstrated unparalleled capabilities in tackling tasks that were once impossible to handle, thus pushing the boundaries of what can be achieved in the realm of artificial intelligence.

Recently, there has been a notable surge in the adoption of deep neural network algorithms by distinguished researchers worldwide, to attend significant obstacles in radar signal processing. The research conducted by Zhe Geng, He Yan, Jindong Zhang, and Daiyin Zhu [38] extensively explores a multitude of deep learning techniques, employed in the domain of radar processing. These techniques, which hold immense potential, are effectively synthesized and visually represented in Figure 4.1, which depicts a comprehensive block diagram that illustrates the most prominent deep learning techniques used in radar processing.

This chapter aims to provide a comprehensive exposition of the theoretical framework underlying the Convolutional Neural Network (CNN), by analysing the fundamental building blocks that are commonly employed in classification tasks. In the context of this thesis, the CNN algorithm serves as the practical algorithm used for the classification of micro Doppler

signatures, exhibited by pedestrians and bicyclists, which lies in the field of Automatic Target Recognition.

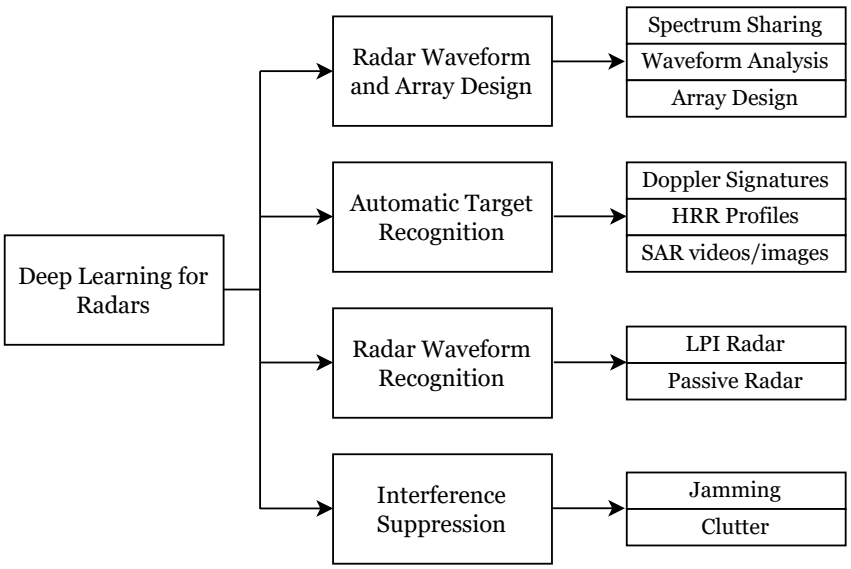

Figure 4.1: Block diagram of the most prominent deep learning techniques used in radar processing, as analyzed in the literature [38].

4.2 Convolutional Neural Networks

A section of the case study of this thesis is dedicated to the classification of Doppler signatures associated with pedestrians and bicyclists. This classification task is accomplished by employing a special type of deep learning algorithm, commonly known as *convolutional neural network* (CNN). A CNN, is a mathematical framework that consists of three main types of layers, which are the building blocks of the network: convolutional layers, pooling layers, and fully connected layers [39]. For in-depth exploration of CNNs and deep learning in general, Phil Kim's work [40] provides extensive analysis and insights into these concepts.

4.2.1 Convolutional Layer

The *Convolutional Layer* is a fundamental component within the CNN architecture, that serves the purpose of feature extraction. It involves a combination of linear and nonlinear operations, specifically the convolution operation and activation function.

Convolution is a specialized linear operation utilized for feature extraction. It involves the application of a small array of numbers, referred to as a *kernel*, across an input array of num-

bers, known as a *tensor*. At each position of the tensor, an element-wise product is computed between each element of the kernel and the corresponding element of the input tensor. These products are then summed to yield the output value, which is placed in the corresponding position of the output tensor. This output tensor is commonly referred to as a *feature map*. An example of this process is illustrated in Figure 4.2. Multiple kernels are employed in this

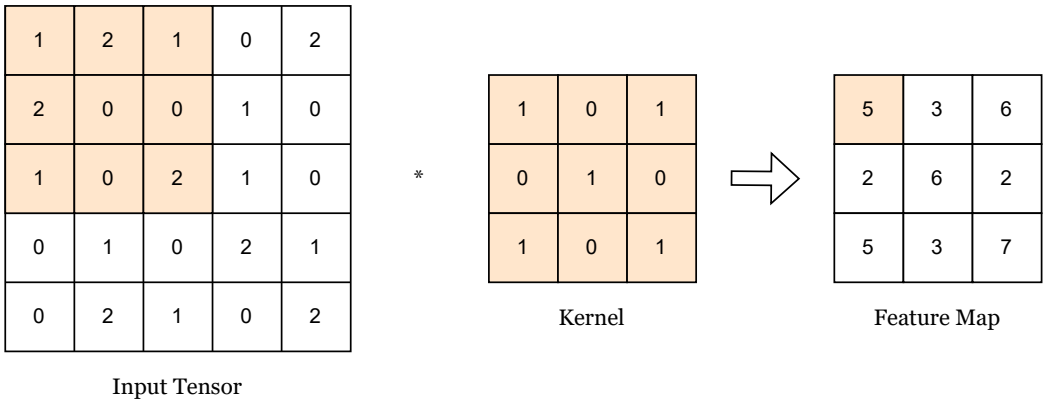

Figure 4.2: An example of the convolution operation with a kernel size of 3×3 [39].

process, generating a variable number of feature maps that represent different characteristics of the input tensors. The convolution operation is defined by two key parameters: the size of the kernel (typically 3×3, but occasionally 5×5 or 7×7) and the number of kernels, which determines the depth of the output feature maps and can vary as desired.

However, the output featured map is reduced in height and width, compared to the input sensor, which would result in successively smaller and smaller feature maps after each convolution operation. This is why the center of each kernel is not allowed to overlap with the outermost element of the input sensor. To address this issue, *padding* is commonly applied, often in the form of zero padding. Zero padding involves adding rows and columns of zeros to each side of the input tensor, allowing the center of a kernel to align with the outermost element and maintaining the same in-plane dimension throughout the convolution operation, as depicted in Figure 4.3. This technique is widely used in modern CNN architectures to preserve in-plane dimensions and facilitate the application of multiple layers.

Another variable that defines the convolution operation the *stride*, which describes the shifting of pixels between two consecutive positions of the kernel. A stride of 1 is commonly chosen, but occasionally, a larger stride is utilized to achieve downsampling of the feature maps. A comprehensive illustration of these operations can be found in the work of Raghuram Vadlamani and Anjali Vishnubhai Patel [41].

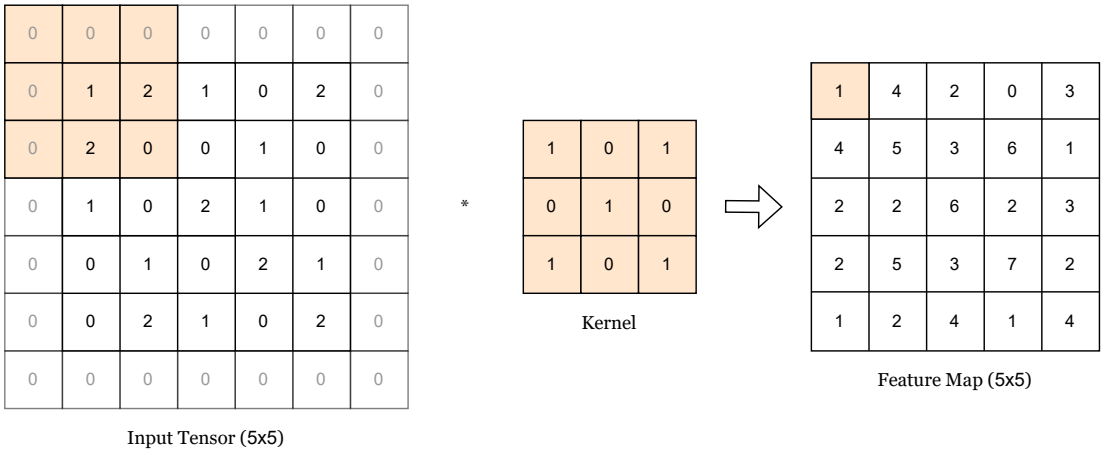

Figure 4.3: An example of the convolution operation with zero padding [39].

The outputs of the convolution operation are then passed through a *nonlinear activation function*. Although smooth nonlinear functions, such as *sigmoid* or *hyperbolic tangent* functions, were used previously because they are mathematical representations of a biological neuron behavior, the most common nonlinear activation function used presently is the *rectified linear unit* (ReLU), a graphical illustration of which is presented in Figure 4.4. The ReLU simply computes the function: $f(x) = max(0, x)$, which converts all the negative values to zero and leaves all the positive values the same.

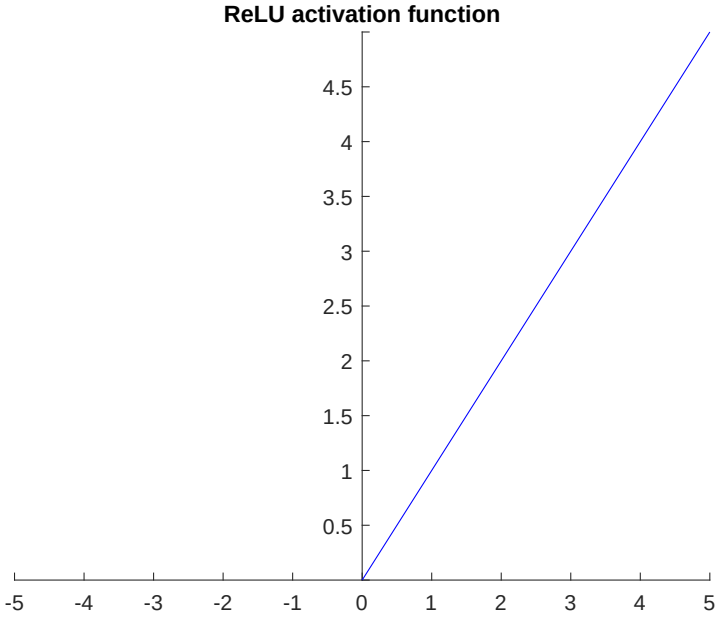

Figure 4.4: Rectified Linear Unit (ReLU) activation function.

In conclusion, an important aspect in training a CNN model, specifically regarding the convolution layer, is to determine the optimal kernels that are most effective for a given

task, based on a provided training dataset. The kernels are the only parameters that are automatically learned during the training process within the convolution layer. However, prior to training, certain parameters such as the size of the kernels, the number of kernels, the padding technique, and the stride value need to be predefined.

4.2.2 Pooling Layer

A pooling layer is a crucial component of a convolutional neural network, that plays a vital role in downsampling the feature maps obtained from the preceding convolutional layers. Its primary objective is to reduce the spatial dimensions of the feature maps, while preserving the most important and relevant information.

To achieve downsampling, the pooling layer partitions the input feature map into non-overlapping regions, usually in the form of squares with a predefined size. Within each region, a pooling operation is performed to summarize the information. The most commonly used pooling operation is *max pooling*, which selects the maximum value within each region and discards the rest. An example of this function is presented in Figure 4.5. This helps to preserve the most prominent features that were present in the region.

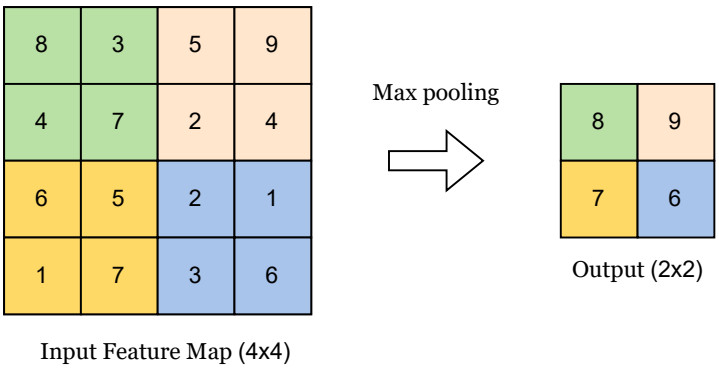

Figure 4.5: An example of the max pooling function with a pooling size of 2×2, no padding, and a stride of 2 [39].

Another pooling procedure worth mentioning is the *global average pooling*. A global average pooling is an extreme type of downsampling in which a feature map of size height$\times$width is downsampled into a 1×1 array, by simply taking the average of all the components in each feature map, while still preserving the depth of the feature maps. This step is normally performed only once before the fully connected layers.

The choice of pooling size and stride in a pooling layer has a direct impact on the degree of the achieved downsampling, and plays a crucial role in shaping the resulting feature maps. The pooling size refers to the dimensions of the pooling regions, commonly represented as 2×2 or 3×3 squares. By selecting a larger pooling size, a more aggressive downsampling is performed, resulting in a greater reduction in spatial dimensions. Conversely, a smaller pooling size leads to a more conservative downsampling approach, retaining more spatial information. In addition to the pooling size, the stride parameter determines the spacing between neighboring pooling regions. Typically, the stride is set to be equal to the pooling size, ensuring non-overlapping regions during the pooling operation. This configuration helps to avoid redundancy and ensures that each region contributes unique information to the downsampling process.

Lastly, it is noteworthy to mention that the pooling layer, to some extent, compensates for eccentric and tilted objects. While the convolutional layer detects objects within an image, the pooling operation aids in determining the location of the object within the image.

4.2.3 Fully Connected Layers

The fully connected layers serve as a mapping mechanism for the extracted and downsampled features. After the feature maps have undergone convolutional and pooling operations, the output of the pooling layer is typically subjected to a transformation known as *flattening*. This process converts the feature maps into a vector representation, allowing them to be used as inputs for one or more fully connected layers. In these fully connected layers, every input neuron is connected to every output neuron through learnable weights. To enhance the performance of the network, these weights are constantly adjusting throughout training. The flattened features, which have been extracted by the convolutional layers and downsampled by the pooling layers, are then passed through these series of fully connected layers. In each fully connected layer, a nonlinear activation function is applied to the outputs. As mentioned previously, the ReLU is a commonly used activation function that introduces non-linearity and helps the network learn complex representations.

The final fully connected layer typically consists of a number of output nodes equal to the number of classes in the classification task. The choice of activation function for this last layer differs from the others and depends on the specific task at hand. For multi-class classification tasks, a popular activation function is the *softmax function*. It normalizes the

output values from the previous layer into target class probabilities, ensuring that each value falls between 0 and 1, and the sum of all values equals 1. This enables the network to provide probabilities for each class, aiding in the final classification decision.

Chapter 5

Case Study

5.1 An Overview of the Case Study

Following this comprehensive review of the literature, it is important to keep in mind that radars used for target detection, tracking and identification, frequently leverage the Doppler shift property, which describes how the frequency of a wave varies, as its source moves relative to the observer. Depending on the direction of the moving target with respect to the radar system, the reflected signals will present a shift in their frequency. For instance, if the target moves towards to the receiver, the reflected waves will be compressed and a rise in their frequency will be expected. This is often referred to as a positive Doppler shift. On the other hand, a target that moves away from the receiver will result in stretching out the reflected waves, inducing a drop in their frequency. This is commonly known as a negative Doppler shift. By analyzing the frequency shift of the reflected waves, the radar system can determine the speed and direction of the target relative to the radar and the extracted information can be later used for a variety of purposes, like detecting the presence of moving vehicles or pedestrians.

However, multiple point objects that move along different directions produce additional frequency modulations that are frequently referred to as *micro – Doppler signatures*. These signatures can then be used to identify targets that consist of multiple moving and distinct parts, such as humans or vehicles, by analysing their respective spectrograms. A spectrogram is a visual representation of the signal strength across a time period at various frequencies that are present in a particular waveform. Each spectrogram provides a unique signature, thus making the classification/identification process feasible. To classify them and extract valu-

able information from them, a properly trained CNN can be employed. There is a lot of work done in this field that leverages these signatures, including “WiSee” [42], a novel gesture recognition system that leverages wireless signals (e.g., WiFi) to enable whole-home sensing and recognition of human gestures, “E-eyes” [43], an approach that senses and identifies fine-grained WiFi signal changes when an activity is performed, “MARS” [44], an assistive rehabilitation system that tracks a patient’s movement using a low-cost mmWave radar.

It is noteworthy to mention that the observed Doppler signatures represent frequency modulations within the radar waveform, which is emitted by an active radar system and scattered in various directions upon encountering a moving target. Subsequent sections will demonstrate that these scattered waveforms can also be captured by passive receivers, as indicated in the work of Vishwakarma et al. (2021) [45]. If such receivers suspect that the received signal potentially contains signatures of individuals present within a specific location, such as a room, they can employ a classification algorithm to identify them. This situation introduces a significant concern regarding individuals’ privacy.

Accordingly, the objective of this thesis is to develop methodologies that obscure the transmitted radar waveform, in order to prevent unauthorized receivers from deciphering the echoes carrying these signatures, thus enhancing the sense of security and privacy for individuals.

5.2 Simulation Setup

To initiate the search for methods aimed at obfuscating human wireless micro-Doppler signatures, in order to prevent passive human activity classification, the first step is to set up the grounds for the simulation. The simulation will be built upon the foundation of an established project developed by MathWorks, titled “Pedestrian and Bicyclist Classification Using Deep Learning” [46]. This project is a complete example that demonstrates how to train and use a Convolutional Neural Network (CNN) to classify moving pedestrians and bicyclists, based on their micro – Doppler characteristics. It also includes car objects, but they are considered as noise sources, thus they will be ignored in this study. The project is built using MATLAB, and it includes the Deep Learning, Signal Processing and Radar Toolboxes.

5.2.1 Layout

The project commences with data generation and preparation. Firstly, radar returns are reflected signals from walking pedestrians and moving bicyclists. The pedestrian walking model [47] coordinates the movement of 16 body segments, imitating natural motion, and simulates the radar reflectivity of each body segment. The moving bicyclist model [48] creates an object consisting of both the bicycle and its rider, and the motion of the object is simulated. Then, the sum of all the reflected signals from numerous distinct scatterers located on the object is computed. Afterwards, by calculating the Short-Time Fourier Transform (STFT) of each radar return, the corresponding micro-Doppler signatures are generated. In the experiments, it was assumed that a monostatic radar model was used, with the active radar being fixed at its origin and the targeted objects being uniformly distributed in a rectangular area of [5,45] and [–10,10] meters along the X and Y axes, respectively, as indicated in Figure 5.1.

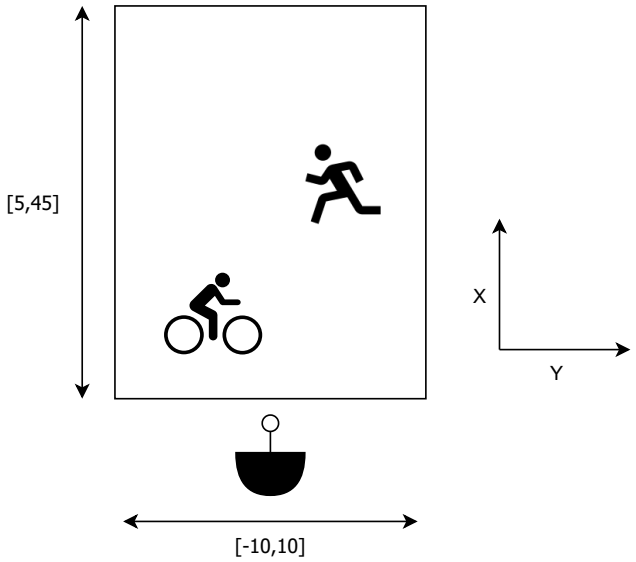

Figure 5.1: The layout plan. The targeted objects are moving strictly inside this rectangular area [46].

5.2.2 Data Preparation

To generate spectrogram illustrations of the pedestrian and the bicyclist, and prior to proceeding with the obfuscation methods, the simulation will be executed twice. One simulation run will focus on a single pedestrian, while the other will specifically consider a single bicyclist.

The stationary radar transmits an FMCW waveform at 24 GHz, with a bandwidth of 250 MHz, a sampling rate of 500 MHz, and of 1 μsec duration. On the 1st experiment, the sole pedestrian is initially located at $[22.00, 4.00]$ m, that moves at a speed of 1.3 m/s, with an initial orientation of 140 degrees, measured from the x-axis towards the y-axis. On the 2nd experiment, a single bicyclist is present in the area, that starts at $[10.00, -4.00]$ m and heads at -30 degrees, at a constant speed of 4.5 m/s. All the tunable parameters for these two objects are presented in Tables 5.1 and 5.2:

Table 5.1: Tunable parameters for the pedestrian object.

Parameters	**Pedestrian**	**Acceptable values**
Height	1.7 m	$[1.5, 2]$ m
Speed	1.3 m/s	$[0, 1.4\text{Height}]$ m/s
Heading	$140°$	$[-180°, 180°]$
Location	$[22, 4, 0]$ m	$[[5, 45], [-10, 10], 0]$ m

Table 5.2: Tunable parameters for the bicyclist object.

Parameters	**Bicyclist**	**Acceptable values**
Speed	4.5 m/s	$[1, 10]$ m/s
Heading	$-30°$	$[-180°, 180°]$
Location	$[10, -4, 0]$ m	$[[5, 45], [-10, 10], 0]$ m
Gear Transmission Ratio	4	$[0.5, 6]$
Pedaling or Coasting	Pedaling	50% Pedaling, 50% Coasting

After generating the reflected signals from both experiments, an STFT algorithm is applied to create the desired spectrograms. As shown in Figure 5.2, the computed spectrograms

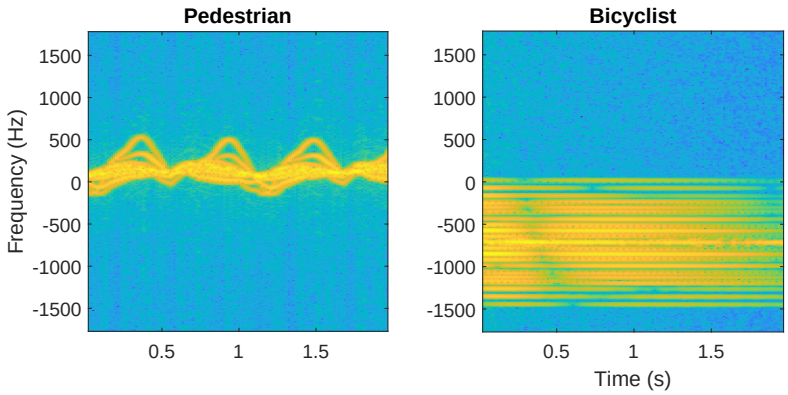

Figure 5.2: The spectrograms of a walking pedestrian (left) and a moving bicyclist (right). The Doppler signatures between these two objects are quite dissimilar.

of the pedestrian (left) and the bicyclist (right) exhibit quite distinct signatures.

In particular, these spectrograms exhibit rich micro-Doppler signatures resulting from distinct movements such as the swinging of arms and legs for pedestrians, and the rotation of wheels for bicyclists. Notably, the spectrograms of each category showcase discernible dissimilarities, highlighting the uniqueness of the generated Doppler signatures.

It is possible to combine the experiments for detecting pedestrians and bicyclists into a single experiment. In scenarios where multiple objects coexist within the radar's detection region, the radar returns encompass a summation of the detected signals, emanating from all objects present. Below, a new set of parameters is presented, which will be applied to create a second realization of a pedestrian and a bicyclist.

Table 5.3: Tunable parameters for the second pedestrian object.

Parameters	**Pedestrian**	**Acceptable values**
Height	1.6 m	$[1.5, 2]$ m
Speed	1.4 m/s	$[0, 1.4\text{Height}]$ m/s
Heading	$110°$	$[-180°, 180°]$
Location	$[26, -3, 0]$ m	$[[5, 45], [-10, 10], 0]$ m

Table 5.4: Tunable parameters for the second bicyclist object.

Parameters	**Bicyclist**	**Acceptable values**
Speed	6 m/s	$[1, 10]$ m/s
Heading	$-40°$	$[-180°, 180°]$
Location	$[15, 1, 0]$ m	$[[5, 45], [-10, 10], 0]$ m
Gear Transmission Ratio	5	$[0.5, 6]$
Pedaling or Coasting	Pedaling	50% Pedaling, 50% Coasting

Figure 5.3 provides a display of spectrograms, representing various combinations of pedestrians and bicyclists, further augmented by the addition of Gaussian background noise. In order to accurately generate these spectrograms, the parameters presented in Tables 5.3 and 5.4 were used, to generate a second realization of one pedestrian and one bicyclist. The spectrogram on the right-hand side was generated using the first realization of the pedestrian and bicyclist object, but other combinations are also feasible (e.g., using the first realization of the pedestrian and the second of the bicyclist, or the second realization of both objects).

Classifying a single realization as either a pedestrian or a bicyclist is fairly straightforward, since both objects have distinct and unique Doppler signatures. However, in cases where the objects overlap, like the one presented in Figure 5.3, distinguishing between multiple objects can be challenging.

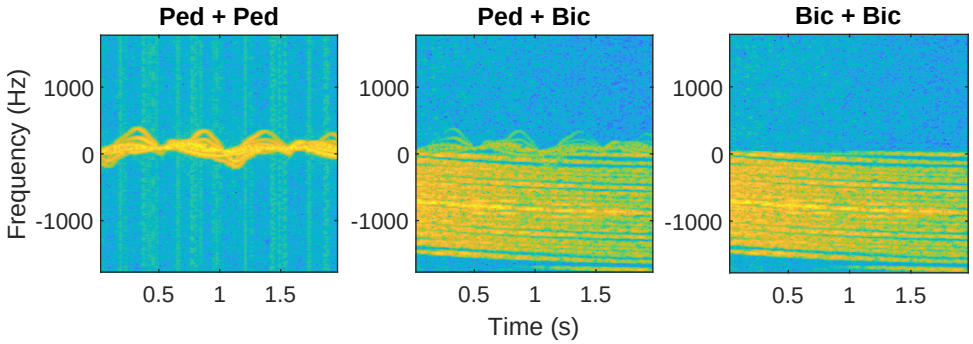

Figure 5.3: The spectrograms of two walking pedestrians (left), one walking pedestrian and one moving bicyclist (middle) and two moving bicyclists (right). In this occasion the pedestrian and bicyclist signatures overlap in both time and frequency.

5.2.3 Creation of a CNN

The next step involved the development of a deep learning model that could differentiate between a bicyclist, a pedestrian, or a combination thereof, based on an input spectrogram. A Convolutional Neural Network (CNN) was chosen for this project, that accepts an image as input and generates a probability of its content. The input images were labeled as containing either a pedestrian, a bicyclist, two pedestrians, two bicyclists, or a combination of one pedestrian and one bicyclist.

The CNN architecture implemented in this case was comprised of five convolutional layers, followed by pooling layers, a fully connected layer, and a softmax layer. The first four convolutional layers were succeeded by a batch normalization layer, a rectified linear unit (ReLU) activation layer, and a max pooling layer. In the final convolutional layer, the max pooling layer was substituted with an average pooling layer. The output layer was a classification layer that used softmax activation.

5.2.4 Network Training and Classification Parameters

For CNN training purposes, a pre-existing dataset containing 10,000 pedestrian and 10,000 bicyclist signals was employed [46]. These signals were merged, followed by the addition of Gaussian noise and the computation of their micro-Doppler signatures, resulting in 5,000 signatures per classification category (either a pedestrian, a bicyclist, two pedestrians, two bicyclists, or a combination of one pedestrian and one bicyclist). 80% of these (4,000 signatures) were allocated for the training dataset, while 20% (1,000 signatures) were reserved

for the test dataset across all categories. The spectrograms fed into the neural network are presented in decibels and normalized to fit within the range of [0,1]. As certain returns may be significantly stronger than others, stronger signals can mask weaker ones, resulting in difficulties for analysis. To tackle this issue, logarithmic scaling (dB) is applied to enhance the features and create a fairer comparison between the received signals. In addition, amplitude normalization aids the CNN into converging more rapidly.

The specified neural network was trained on an HP laptop with an AMD Ryzen 5 3500U with Radeon Vega Mobile Gfx 2.10 GHz CPU, utilizing the parameters outlined in [46]. The only alteration made was that a CPU was used instead of a GPU. Through this training method, an accuracy of nearly 86% was achieved over 30 epochs. The results extracted from the confusion matrix are displayed in Table 5.5, offering a detailed analysis of the prediction accuracy for each category. The matrix demonstrates that the network accurately predicts the labels of the signals in the existing test dataset across all different scenarios with high accuracy.

Table 5.5: The prediction results for the 5 different scenarios. The table demonstrates that the average detection and classification accuracy for each category is rather high.

Scenario	Accuracy
Pedestrian	91.7%
Bicyclist	93.6%
Pedestrian + Bicyclist	76%
Pedestrian + Pedestrian	85%
Bicyclist + Bicyclist	83.4%
Overall	**86**%

5.2.5 Concerns

A moving object, targeted by an active radar, becomes a virtual transmitter that reflects the emitted radiation. While the active radar receives the echoes for further processing, an unauthorized receiver, such as a passive radar, can also detect the scattered radiation [49]. Though the passive radar lacks knowledge of the active radar's operating parameters and modulation techniques, it can still receive the signal. Conducting the same experiments as indicated in Section 5.2.4, it is demonstrated that by applying an STFT to the received, non-demodulated signals, the produced spectrograms almost perfectly resemble those obtained

by the active radar, as demonstrated in Figure 5.4. This raises significant privacy concerns for the targeted individuals.

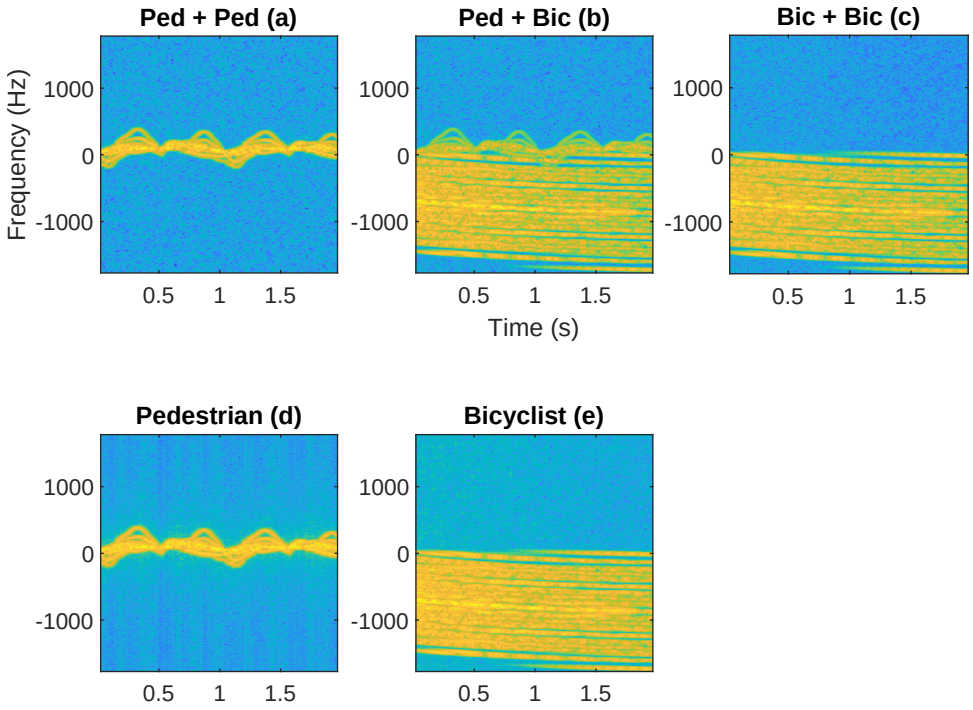

Figure 5.4: The produced spectrograms of two walking pedestrians (a), one walking pedestrian and one moving bicyclist (b), two moving bicyclists (c), one walking pedestrian (d) and one moving bicyclist (e). The distinct features for each scenario almost perfectly resemble those illustrated in Figures 5.3 and 5.2, respectively.

To further investigate the matter, two datasets were generated, where each of those consisted of 200 pedestrian and 200 bicyclist objects, using the steps outlined in Section 5.2.2. However, for the simulations this time, the waveform's bandwidth was decreased to 20 MHz, resulting in a lower sampling rate of 40 MHz. Although this change was made for efficiency reasons, the resulting spectrograms still exhibit the same unique characteristics that are necessary for the CNN to classify properly. It is important to note that the only difference between the first and second datasets is that in the former, the signals reflected from the simulated objects were processed at the active radar receiver, while the latter only includes the scattered radiation an unauthorized receiver can collect.

Active Radar

The first dataset used in this study included various categories of objects, namely "pedestrian", "bicyclist", "pedestrian + pedestrian", "pedestrian + bicyclist", and "bicyclist + bicy-

clist". To classify this dataset, the trained network from Section 5.2.4 was employed. However, it is worth noting that the categories "pedestrian + pedestrian" and "bicyclist + bicyclist" consisted of only 100 spectrograms each, instead of the usual 200, as the objects were merged, leading to a reduced dataset. The results of the classification process are shown in Table 5.6, with an average accuracy of 76.9%. The outcome extracted from the confusion matrix indicates that the trained network performed much better in predicting scenes with multiple objects.

Table 5.6: The resulting predictions of the confusion matrix for the active radar. Most prediction errors occur when the network classifies the "pedestrian" object as "pedestrian + pedestrian" or "pedestrian + bicyclist".

Scenario	Accuracy
Pedestrian	56%
Bicyclist	90%
Pedestrian + Bicyclist	80%
Pedestrian + Pedestrian	77.5%
Bicyclist + Bicyclist	81%
Overall	**76.9**%

Passive Radar

Moving on to the second dataset, it contained the same information as the first one, except for the fact that the reflected signals were not processed and demodulated. However, the network was able to successfully identify most of the objects, as demonstrated in Table 5.7, in a similar manner as it did for the first dataset. This implies that the passive radar, despite lacking knowledge about the active radar operating parameters and modulation techniques and while not being able to perform range or Doppler estimation, it can still predict the presence of pedestrians and bicyclists in a room with an impressive accuracy of 73.9%. It is important to note that the accuracy results may differ slightly from user to user due to the network being trained on different computers, but the classification results for each dataset are expected to be relatively consistent.

In conclusion, upon comparing Figures 5.2 and 5.3 with Figure 5.4, it becomes apparent that no significant differences can be discerned, apart from some minor variations in the spectrograms' resolution. This raises a grave concern, as unauthorized devices have the po-

Table 5.7: The resulting predictions for the received signals at the unauthorized receiver. The passive radar can still identify with high accuracy the presence of an object in a room.

Scenario	Accuracy
Pedestrian	58%
Bicyclist	73.5%
Pedestrian + Bicyclist	80%
Pedestrian + Pedestrian	76%
Bicyclist + Bicyclist	82%
Overall	**73.9**%

tential to collect the scattered radiation that contains these micro-Doppler signatures, employ classification algorithms based on known patterns, and extract sensitive details regarding the target's identity. Consequently, it is imperative to develop novel methodologies that safeguard the privacy of individuals under surveillance. Of particular interest is the exploration of waveform obfuscation techniques, which, as it is explored in subsequent sections, have proven to be remarkably effective in concealing crucial information from malicious users.

5.3 Obfuscation Techniques

Signal obfuscation is a technique used to deliberately obscure or conceal information contained in a signal, in order to prevent unauthorized access, manipulation or interpretation. In the context of wireless communications, signal obfuscation is often used to protect against eavesdropping, jamming or other forms of interference, ensuring that the signal can only be understood by authorized users who possess the necessary decryption key or other means of deciphering the signal.

5.3.1 Case 1: Obfuscation through Frequency Fluctuations

In Section 5.2.5, it was demonstrated that an unauthorized receiver has the capability to use the reflected signals from a moving target to accurately track and identify it, which poses a major violation of privacy if the individual is unaware of it. So, one potential solution to address this problem is to introduce frequency fluctuations into the transmitted signals, which can obscure these micro – Doppler signatures. This technique has been the subject of extensive research, as highlighted in the work of Argyriou [50], where the insertion of

an artificial, frequency variated signal in the transmitted waveform, so as to alter the real micro-Doppler effects, is investigated.

To successfully obfuscate the micro doppler signatures that reveal the identity of a moving target, an oscillating sinewave was used to encapsulate the emitted signal. In the time domain, this waveform is defined as a frequency modulated (FM) waveform with a maximum instantaneous frequency shift of F_{imax} and a frequency of f_m, resulting in an instantaneous frequency of $F_i(t) = f_c + F_{imax} \cdot \cos(2\pi f_m t)$ [51]. The introduction of this waveform will not affect the demodulation of the digital communication signal at the active receiver. The FM alternated signal is then expressed as:

$$x_{obf}(t) = e^{j\frac{F_{imax}}{f_m}\sin(2pif_m t)} \tag{5.1}$$

This waveform produces in the frequency domain a signal that spreads between the maximum instantaneous frequencies shifts of $-F_{imax}$ to F_{imax}, at a rate of f_m Hz.

The purpose of using the oscillating sinewave as a modulation technique is to obfuscate micro - Doppler signatures in the frequency domain, thereby making it harder to extract information about the target's identity. The frequency at which various human body parts move is typically in the range of a few 10's of Hz, and thus, the maximum instantaneous frequency shift should be around that limit. In previous experiments, the objects were uniformly distributed in a rectangular area, and the other properties were adjusted randomly within specified ranges, as indicated in Tables 5.1 - 5.4. The height of the pedestrian objects was uniformly distributed between 1.5 and 2 meters, resulting in walking speeds ranging from 0 to 1.4 times their height, in meters per second. Therefore, a human with a height of 2 meters would have a maximum speed of 2.8 m/s, resulting in a maximum Doppler shift of 448 Hz. However, since the average walking speed is 1.4 m/s [52], the average Doppler shift is 224 Hz. Taking into consideration that the speed is uniformly distributed in the range of [0, 2.8] m/s, a maximum instantaneous frequency shift F_{imax} of ± 200 Hz is sufficient to smear the received signal spectrograms effectively, as shown in Figure 5.5. The value of f_m, which was set to 10 Hz, is already high enough to cover the moving pedestrian that presents peaks in the spectrograms of Figure 5.2 (left) with a peak-to-peak difference of 0.5 seconds (2 Hz).

5.3.2 Simulation

Figure 5.5 depicts the experiments performed in accordance with Section 5.2.4, utilizing the same parameters. However, this time, the obfuscation technique that was employed in the transmitted signals, for $F_{imax} = \pm 200$ Hz and $f_m = 10$ Hz, resulted in the reflected Doppler returns appearing too abstract, devoid of any distinguishable features that the classification algorithm could identify in the passive receiver.

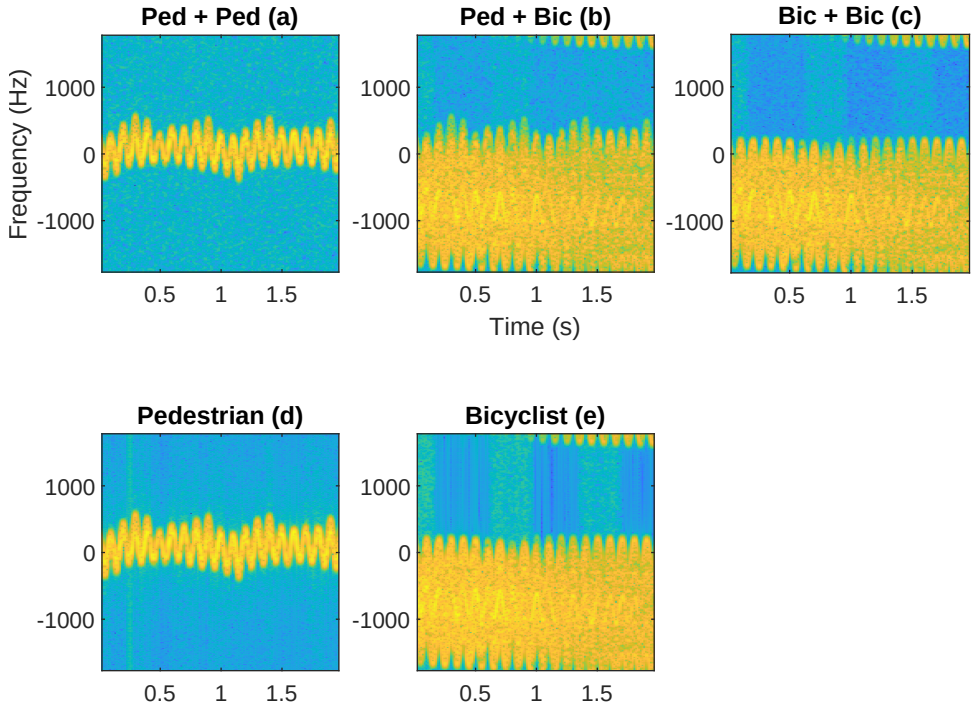

Figure 5.5: The results of the obfuscating technique in the passive receiver, across the five categories of two walking pedestrians (a), one walking pedestrian and one moving bicyclist (b), two moving bicyclists (c), one walking pedestrian (d) and one moving bicyclist (e). It is worth noting that smearing the signals has destroyed the doppler signatures.

To evaluate the impact of obfuscation, a new dataset was created, which consisted of 200 pedestrian and 200 bicyclist objects. The dataset was generated using the same parameters as those used in Section 5.2.5, except for the use of the obfuscating technique. The trained network from Section 5.2.4 was utilized to classify the spectrograms that had been smeared.

5.3.3 Results

In comparison to the 73.9% of accuracy that was achieved in the previous experiment of Section 5.2.5, the classification process this time yielded a significantly lower average

accuracy of 30.75%, as shown in Table 5.8. This table represents the classification predictions for each scenario, extracted from the confusion matrix illustrated in Figure 5.6.

The confusion matrix provides a summary of the classification results. Each row represents the predicted class, and each column corresponds to the true class. The diagonal cells represent the correctly classified observations, while the off-diagonal cells represent the incorrect classifications. The number in each cell indicates the number of observations in that particular category. The column on the right side displays the precision and false discovery rate. The *precision* (in blue colours) represents the percentage of correctly classified examples for each predicted class, while the *false discovery rate* (in red colours) represents the percentage of incorrectly classified examples for each predicted class.

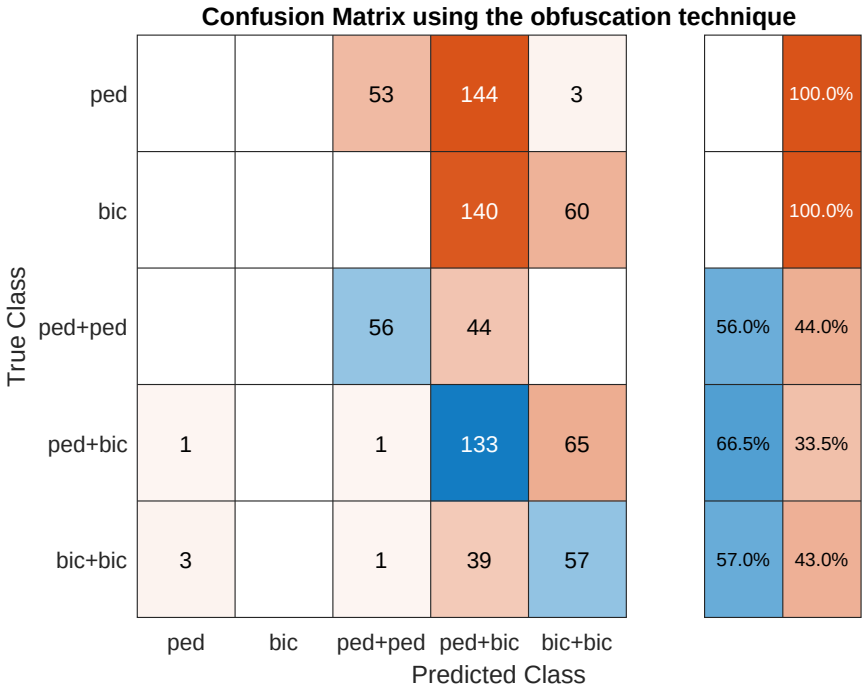

Figure 5.6: The prediction performance of each scenario, when obfuscation is used. In scenarios with multiple targets present, the prediction accuracy is higher.

In the scenarios of a single pedestrian and a single bicyclist, the confusion matrix reveals that many pedestrian objects were falsely identified as a combination of a pedestrian and a bicyclist and sometimes as two pedestrians. Similarly, bicyclist objects often resembled a combination of a pedestrian and a bicyclist or two bicyclists. As a result, there were frequent misclassifications between the ”pedestrian” and ”bicyclist” categories, effectively achieving the intended goal of obfuscation. It is worth noting that, as mentioned in Section 5.2.5, the dataset for scenarios involving two pedestrians or two bicyclists present in the scene, was

created by combining 200 samples of pedestrians and 200 samples of bicyclists. As a result, there were only 100 samples available for these specific scenarios, instead of the original 200 samples.

Table 5.8: Classification results for the smeared data. Even though the passive radar is unable to classify individual objects, it can classify combos of them.

Scenario	Accuracy
Pedestrian	0%
Bicyclist	0%
Pedestrian + Bicyclist	66.5%
Pedestrian + Pedestrian	56%
Bicyclist + Bicyclist	57%
Overall	$\mathbf{30.75}\%$

Nevertheless, the passive receiver can still predict with sufficient accuracy the identity of multiple objects that exist concurrently in the area, particularly in scenarios where a pedestrian and a bicyclist are present together, as indicated in Table 5.8. This is likely due to similarities in the overlapping frequencies between the spectrograms shown in Figure 5.3 (middle) and in Figure 5.5(b). Therefore, the obfuscation technique cannot fully conceal and safeguard the unaware targets.

Hence, it is necessary to explore alternative techniques that offer a diverse range of obfuscation. This aspect is thoroughly examined in Section 5.3.4, where the utilization of a phased array is investigated as a substitute for a single antenna.

For future reference, alternative values were explored for the parameters F_{imax} and f_m before settling on the final choices. For F_{imax} values of 1000, 800, and 500 Hz, the amplitude in the frequency axis exceeded greatly the maximum Doppler shift of 448 Hz for the pedestrian scenario. However, the overall classification outcome remained unaffected, thus, the smallest feasible value F_{imax} = 200 Hz was chosen, which does not affect the classification process. It is worth noting that it is still possible to achieve similar results, even with higher values of F_{imax}.

On the other hand, when using f_m values below 10 Hz, it was noticed during the study that the waveform along the time axis does not exhibit significant alterations, allowing the passive receiver's classifier to still identify scenarios with single pedestrians or bicyclists accurately. Values higher than 10 Hz resulted in an excessive number of spikes, which adversely affected

the classification process. However, values up to $f_m = 15$ Hz do not impact the classification accuracy.

5.3.4 Case 2: Obfuscation Through Phased Arrays

An alternative approach that disrupts the accurate extraction of micro-Doppler signatures at the receiver, when intentionally desired by the transmitter, involves the utilization of phased arrays. The underlying concept is that the resulting spectrograms, will exhibit different patterns compared to those examined in Sections 5.2.2 and 5.2.5, if certain array elements are turned off while others remain active during specific time stamps. By periodically altering the geometry of the phased array, the radiated signal can be effectively obfuscated. This means that the characteristics of the signal, including the micro-Doppler signatures, will undergo multiple disruptions at regular intervals. Thus, the task of extracting valuable information from the transmitted signal can become significantly more challenging for passive receivers.

5.3.5 Phased Array Setup

The experimental setup, described in Section 5.2.2, has been upgraded to include phased arrays for both the transmission and reception of signals in the active radar system, as depicted in Figure 5.7. By employing phased arrays, the radar system gains the capability to dynamically adjust the geometry and configuration of the antenna elements, as well as to better manipulate and control the transmitted and reflected signals.

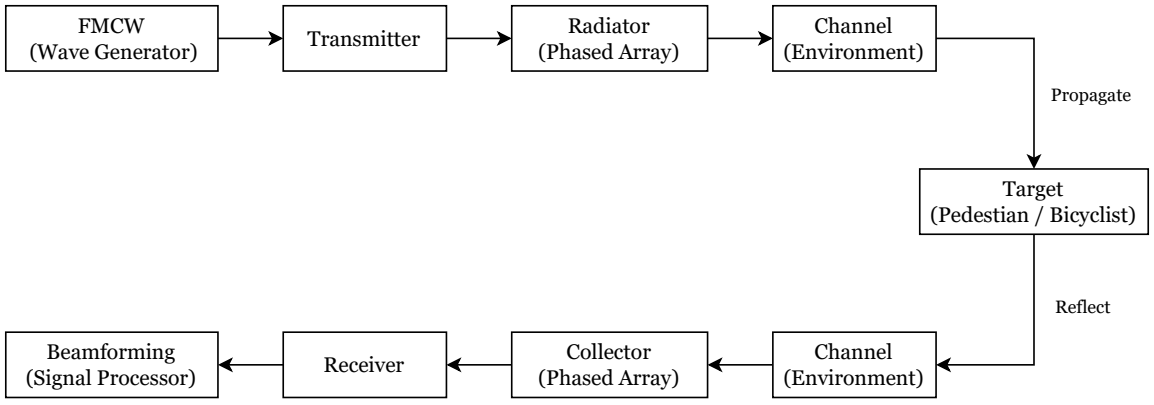

Figure 5.7: Upgraded setup, employing phased arrays for transmission and reception of signals in the active radar system.

In this study, a Uniform Linear Array (ULA) configuration was selected, although other

configurations could also be suitable. The ULA consists of 30 isotropic antennas, each uniformly radiating in all directions. As explained in Section 3.8.1, by increasing the number of isotropic antennas in the linear array, the produced interference pattern will lead to a more concentrated and directional central beam. For this reason, the use of a ULA enables electronic beam steering, allowing the direction of the beam to be adjusted rapidly.

Array Configuration

In order to implement the idea of selectively turning on and off elements of the array at specific time intervals, various configurations were experimented with. Among these configurations, one particular pattern has shown promising results and is described as follows:

1. In the beginning of the simulation, the first 15 elements (1 to 15) of the array are turned on, where each element is separated by $\frac{\lambda}{2}$.

2. In each time interval T_{samp}, the subsequent element in the array is turned on, while the 1st turned on element in the sub-array is turned off. For example, if the first 15 elements are initially on, then, during the second time interval, the 16th element will be turned on, and the 1st element will be turned off. This pattern of turning on and off elements continues in a consecutive manner.

3. After the last element (30th) of the array is turned on, the process will reverse, resulting in the last turned on element being turned off, and the element preceding the 1st turned on element of the sub-array being turned on. For example, if in a specific time interval the elements 16 to 30 are on, then in the next time interval the elements 15 to 29 will be on. This pattern of backward progression ensures the cyclic operation of turning on and off elements within the array.

4. Steps 2 and 3 are repeated until the simulation is completed.

5.3.6 Simulation

Before conducting extensive tests on various datasets, it is necessary to examine how the new array configuration distorts the micro-Doppler signatures for the moving pedestrians and bicyclists, in both the active and passive receivers. In order to accomplish this, the simulation will be firstly executed for two scenarios, where the first one involves a moving pedestrian

and the second one a moving bicyclist. The tunable parameters of the targeted objects are outlined in Tables 5.9 and 5.10, respectively. In Figure 5.8, noticeable discrepancies can

Table 5.9: Tunable parameters for the pedestrian object.

Parameters	**Pedestrian**	**Acceptable values**
Height	2 m	$[1.5, 2]$ m
Speed	2 m/s	$[0, 1.4\text{Height}]$ m/s
Heading	$-150°$	$[-180°, 180°]$
Location	$[13.8, 7.5, 0]$ m	$[[5, 45], [-10, 10], 0]$ m

Table 5.10: Tunable parameters for the bicyclist object.

Parameters	**Bicyclist**	**Acceptable values**
Speed	4.5 m/s	$[1, 10]$ m/s
Heading	$-30°$	$[-180°, 180°]$
Location	$[10, -4, 0]$ m	$[[5, 45], [-10, 10], 0]$ m
Gear Transmission Ratio	5	$[0.5, 6]$
Pedaling or Coasting	Pedaling	50% Pedaling, 50% Coasting

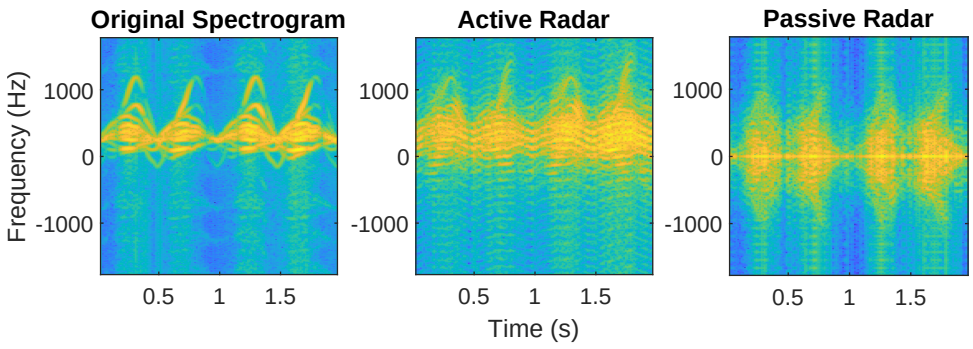

Figure 5.8: The spectrograms of a walking pedestrian, under the new array configuration. The left subplot depicts the doppler signature of the pedestrian, had the configuration been the original one, while the centered and right subplots illustrate the resulting signatures the active and passive receivers produce, respectively.

be observed in the resulting signatures, obtained from both the active and passive radars. These differences arise due to the rapid and dynamic changes that take place in the array configuration, throughout the simulation. The left subplot serves as a reference, so that to assess the impact of turning off and on the array elements on the Doppler signatures.

While the signatures in the active radar bear resemblance to the ones depicted in the left subplot, it was observed during the simulations that these signatures exhibit a strong correlation with the pedestrian's position and heading direction. Consequently, if for example

the heading direction is altered to $100°$, it will lead to discernible deviations from the original spectrograms, potentially impacting the classification procedure. Figure 5.9 presents the distorted spectrograms.

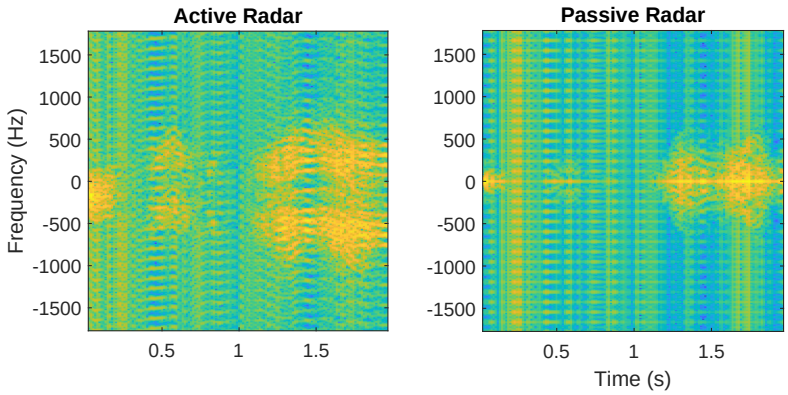

Figure 5.9: The spectrograms of a walking pedestrian, if the heading direction is changed to the random value of $100°$. It is evident that the resulting signatures are highly dependent on the heading direction of the moving target.

On the other hand, in order for the passive receiver to accurately decode the reflected signals that traverse the wireless medium, it is crucial to have knowledge of the channel's propagation characteristics. These characteristics are encapsulated by the term "Channel State Information" (CSI) [53], which provides valuable insights into how a signal propagates from the transmitter to the receiver, enabling a better understanding of the channel's behavior.

In the frequency domain, the relationship between the transmitted signal $X(f_c, t)$ and the received signal $Y(f_c, t)$, with f_c denoting the carrier frequency, can be expressed as follows:

$$Y(f_c, t) = H(f_c, t) \cdot X(f_c, t), \tag{5.2}$$

where $H(f_c, t)$ is the Channel Frequency Response (CFR), measured at time t. The use of CSI estimates for calculating the Doppler spectrogram at the passive receiver is crucial in this simulation, considering that the channel conditions change rapidly and that the CSI measurements are sensitive to the surrounding environment and the RF reflections from the human body [54]. As mentioned in this chapter, these reflections produce distinct frequencies/signatures, depending on the activities being performed. To analyze these frequencies in the time-frequency domain, an STFT is applied to the received signal. The STFT divides the signal into equally-sized segments using a sliding window, and performs a FFT on each segment.

However, since human movements introduce frequency fluctuations that impinge on the reflected signal, then these fluctuations create variations at the power of the received signal over certain frequency bands, meaning that the CFR is affected. For this reason, by squaring the CFR, which is contained in the CSI measurements, the magnitude/power of the channel response can be captured. This squared CFR is then used to calculate the spectrogram of the signal.

The resulting spectrogram, as shown in the right subplot of Figure 5.8, demonstrates the effectiveness of employing this method for obfuscating the transmitting signal. The differences between the produced spectrogram and the reference spectrogram validate the ability of the array variations to successfully distort the signal.

Applying the same approach as described above, the spectrograms obtained from the second scenario involving a single moving bicyclist are depicted in Figure 5.10. Similar to the previous case, notable alterations can be observed in the Doppler signature of the passive receiver. This demonstrates the effectiveness of the method in obfuscating the transmitting signals by leveraging the physical properties of the array. The significant changes in the Doppler signature further validate the potential of this technique for enhancing privacy and security in radar communication.

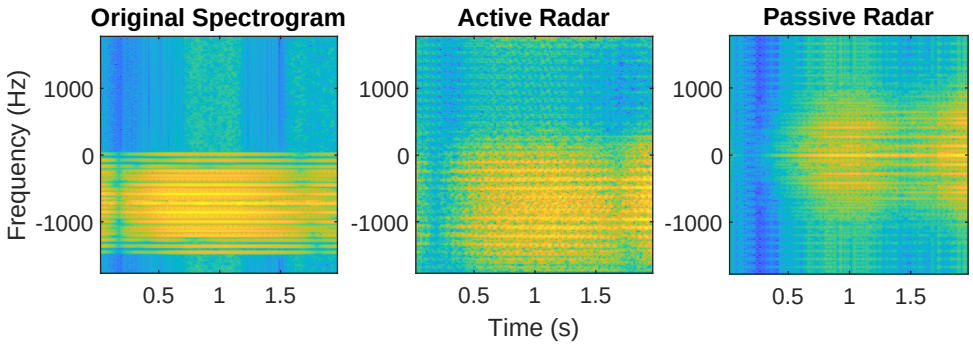

Figure 5.10: The spectrograms of a moving bicyclist, under the new array configuration. The left subplot depicts the doppler signature of the bicyclist, had the configuration been the original one, while the centered and right subplots illustrate the resulting signatures the active and passive receivers produce, respectively.

To assess the effectiveness of this particular obfuscation technique, a new dataset comprising of 200 pedestrian and 200 bicyclist objects was generated. The dataset parameters were adjusted to align with the setup described in Section 5.3.5, while being consistent with the parameters used in Section 5.2.5. In this evaluation, the spectrograms generated by both

the active and passive receivers were classified using the previously trained network from Section 5.2.4. It is important to note that this obfuscation technique impacts the classification performance of the active receiver as well, warranting its evaluation in this context.

5.3.7 Results

The classification process for Case 2 exhibited an average accuracy of only 9.88% at the passive receiver. In comparison to the results discussed in Section 5.3.3, in which the experiments of Case 1 had yielded an average accuracy of 30.75%, it becomes apparent how remarkably effective this specific technique is in concealing micro-Doppler signatures from unauthorized users, just by leveraging the physical properties of the phased array. Table 5.11 indicates that the network fails to accurately predict scenarios involving a single pedestrian or a single bicyclist, successfully accomplishing the intended goal of obfuscation. Furthermore, in scenarios with multiple objects, the passive receiver's predictions regarding the identity of these objects lack of any significant accuracy, thus demonstrating the obfuscation of the resulting signatures obtained from all scenarios is sufficient. In contrast, Case 1 could only effectively obfuscate signatures representing sole objects.

Table 5.11: The resulting predictions for the received signals at the passive receiver. The passive radar can no longer identify with high accuracy the presence of an object in a room.

Scenario	Accuracy
Pedestrian	0.5%
Bicyclist	0%
Pedestrian + Bicyclist	15%
Pedestrian + Pedestrian	12%
Bicyclist + Bicyclist	36%
Overall	**9.88%**

Nevertheless, as stated earlier, this approach impacts the classification procedure in the active receiver by introducing some degree of alteration to the resulting signatures. The predictions of the trained neural network at the active receiver, illustrated in Table 5.12, exhibit a prediction accuracy of merely 18.75%. This accuracy is significantly lower compared to the 76.9% achieved in Section 5.2.5, indicating that this technique is sub-optimal when classification in the active receiver is necessary.

A way to improve the ability of the active receiver to classify the targeted objects more ef-

Table 5.12: The resulting predictions for the received signals at the active receiver. The active radar struggles to identify with high accuracy the presence of a target in a room, due to the impact of obfuscation in the resulting signatures.

Scenario	Accuracy
Pedestrian	22%
Bicyclist	1.5%
Pedestrian + Bicyclist	15.5%
Pedestrian + Pedestrian	7%
Bicyclist + Bicyclist	65%
Overall	$\mathbf{18.75}\%$

fectively is by slightly modifying the Phased Array Setup, described in Section 5.3.5. Instead of activating and deactivating the array elements at each time interval T_{samp}, the alternation can occur every $100T_{samps}$. Through simulations, it was observed that while the spectrograms in the passive receiver remained obfuscated to the same extent as in the original planar configuration, the spectrograms in the active receiver exhibited improvement. This observation is further supported by the analysis of Tables 5.13 and 5.14.

Table 5.13: The new predictions for the received signals at the active receiver, employing the updated configuration. In this setup, the active radar can identify with better accuracy the presence of an object in a room, in comparison to the predictions depicted in Table 5.12.

Scenario	Accuracy
Pedestrian	43.5%
Bicyclist	10%
Pedestrian + Bicyclist	51%
Pedestrian + Pedestrian	78%
Bicyclist + Bicyclist	33%
Overall	$\mathbf{40}\%$

According to the findings presented in Table 5.13, the active radar system now demonstrates an improved ability to accurately predict scenarios involving pedestrians in the scene. This improvement is evident in the overall accuracy, which has increased to 40%. This represents a significant advancement compared to the results depicted in Table 5.12, where the overall accuracy was only 18.75%. On the other hand, as indicated in Table 5.14, the overall accuracy of 9% at the passive receiver suggests that the obfuscated signatures are not really influenced by this new alteration. This observation aligns with the results presented in Table

5.11, thus the resulting accuracy remains at a low of 9 - 10%.

Table 5.14: The new predictions for the received signals at the passive receiver, employing the updated configuration. In this setup, the passive radar still struggles to correctly predict the identity of the targeted object.

Scenario	Accuracy
Pedestrian	5%
Bicyclist	0%
Pedestrian + Bicyclist	8%
Pedestrian + Pedestrian	17%
Bicyclist + Bicyclist	29%
Overall	**9**%

Chapter 6

Discussion

Radar technology plays a crucial role in various aspects of human life, offering numerous applications and advantages. Unlike other sensing technologies, radars excel in operating effectively across both short and long distances, even under challenging environmental conditions. They possess the unique capability to penetrate non-conductive materials, such as walls, thus enabling the detection and localization of objects on the other side. This particular aspect of radar ability is currently an active and extensively studied area of research. When a radar waveform is transmitted through a wireless channel and interacts with a moving target, composed of multiple parts that move in various directions, the resulting reflected signal exhibits distinct frequency shifts known as micro-Doppler signatures. Spectrograms serve as an effective representation and analysis method for these signatures. By inputting these spectrograms into a neural network, trained for this purpose, the network can recognize the target's identity and the specific activity being performed, based on the patterns formed by these signatures. However, the inherent characteristics of the wireless channel allows unauthorized users to intercept the reflected signals that contain these signatures. By employing a classification algorithm, they can also accurately determine the identities of these targets. This situation gives rise to significant privacy concerns regarding the targeted individuals.

The objective of this thesis was to investigate efficient techniques for obfuscating these micro-Doppler characteristics, aiming to hinder their interpretation by malicious users. In particular, two obfuscation techniques were examined, in a simulated environment where the targets were moving pedestrians or moving bicyclists. The first technique involved applying a frequency variated signal to an FMCW transmitting waveform, and the second one utilized a phased array system, strategically toggling the activation and deactivation of specific

elements to alter the resulting micro-Doppler characteristics. These methods were evaluated across five distinct scenarios, which included a single moving pedestrian, a single moving bicyclist, two moving pedestrians, two moving bicyclists, as well as the simultaneous presence of a moving pedestrian and a moving bicyclist within the same scene. To further test the accuracy of these methods, a pre-trained Convolutional Neural Network was utilized to classify 200 sample data of pedestrians and 200 sample data of bicyclists, across all five scenarios, by running the classifier at both the active radar and the unauthorized receiver.

6.1 Conclusion

Both approaches demonstrated promising results in terms of obfuscating these micro-Doppler signatures. Comparing the classifier's predictions from a simulation run without utilizing these techniques (76.9% for the active radar and 73.9% for the passive receiver), the updated predictions are as follows:

Case 1

The first technique, that involved encapsulating an oscillating sinewave to the transmitting waveform, resulted in a prediction rate of 30.75% for the passive receiver. In comparison to the referenced prediction rate of 73.9%, this represents an acceptable level. For scenarios where there is only one pedestrian or one bicyclist present, the prediction rate is 0%, which is optimal. However, in other scenarios with multiple targets, the prediction rate exceeds 50% for each scenario, suggesting that this technique may not be suitable in such cases. For the active receiver, as the added waveform is known and can be easily subtracted, the prediction rate remains unaffected.

Case 2

The second technique, which utilized the physical properties of the phased array system to alter the micro-Doppler characteristics, demonstrated a remarkably low accuracy of only 9.88%. In scenarios involving single pedestrians and single bicyclists, the prediction rate nearly approached 0%. In cases where two pedestrians or one pedestrian and one bicyclist were present concurrently, the prediction rate remained at around 15% for each case. However, for the scenario with two bicyclists, the prediction rate reached 36%, indicating that

this technique may not be ideal when multiple bicyclists are present. However, it is important to note that this method also impacts the classification process in the active receiver. The prediction results revealed an overall accuracy of only 18.75%, which is sub-optimal when reliable classification is required in the active receiver. Specifically, the prediction rate for a single pedestrian is 22%, while for a bicyclist, it is only 1.5%. These effects extend to scenarios involving multiple objects, with accurate predictions of two pedestrians at only 7%, one pedestrian and one bicyclist at 15.5%, and two bicyclists at 65%.

To address the issue of low accuracy in the active receiver, by reducing the rate at which the array elements are activated and deactivated, it was concluded that while the overall results in the passive receiver did not exhibit significant changes, there was a remarkable improvement in the predictions at the active radar. Now, the overall accuracy in the passive receiver stands at 9%. While in the bicyclist scenario the accuracy remained at 0%, for the pedestrian scenario it increased to 5%. In cases where multiple objects were present, the prediction rate for two bicyclists decreased to 29%, while for the combination of a pedestrian and a bicyclist, it decreased to 8%. However, in the scenario involving two pedestrians, the prediction rate increased to 17%. On the other hand, the active radar exhibited a significant improvement in accuracy, reaching 40%. In the pedestrian scenario, the accuracy percentage doubled, while for the bicyclist scenario, it reached 10%. Notably, the accuracy prediction for two pedestrians reached an impressive 77%, and for the combination of one pedestrian and one bicyclist, it reached 51%, indicating that this technique is effective when pedestrians are present in the scene. However, in the scenario involving two bicyclists, the prediction percentage decreased to 33%.

6.2 Future Work

In summary, both techniques are effective in obfuscating radar waveforms to hinder passive human activity classification. The first technique greatly reduces the recognition of pedestrians and bicyclists, but it requires modifying the transmitting waveform and employing additional signal processing techniques to restore the original waveform at the active receiver. On the other hand, the second technique achieves obfuscation by manipulating the array geometry, without the need for waveform alteration. However, the classification process in the active receiver is also affected by this technique, resulting in a decreased prediction

accuracy.

For future reference, it is worth considering experimenting with alternative phased array setups that could potentially improve the prediction results for both the passive and active receiver.

Bibliography

[1] Aryan Kaushik, Evangelos Vlachos, John Thompson, Maziar Nekovee, and Fraser Coutts. Towards 6g: Spectrally efficient joint radar and communication with radio frequency selection, interference and hardware impairments (invited paper). *IET Signal Processing*, 16(7):851–863, 2022.

[2] Fan Liu, Christos Masouros, Athina P. Petropulu, Hugh Griffiths, and Lajos Hanzo. Joint radar and communication design: Applications, state-of-the-art, and the road ahead. *IEEE Transactions on Communications*, 68(6):3834–3862, 2020.

[3] Luo Feu. Human activity classification using micro-doppler signatures and ranging techniques. School of Electronic Engineering and Computer Science Queen Mary, University of London, United Kingdom, January 2020.

[4] Lingyun Ren, Tran Nghia, Haofei Wang, Aly Fathy, and Ozlem Kilic. Analysis of micro-doppler signatures for vital sign detection using uwb impulse doppler radar. In *IEEE Topical Conference on Biomedical Wireless Technologies, Networks, and Sensing Systems (BioWireleSS)*, pages 18–21, 01 2016.

[5] Youngwook Kim and Brian Toomajian. Hand gesture recognition using micro-doppler signatures with convolutional neural network. *IEEE Access*, 4:7125–7130, 2016.

[6] Harish Chandra Kumawat, Mainak Chakraborty, A. Arockia Bazil Raj, and Sunita Vikrant Dhavale. Diat-µsat: micro-doppler signature dataset of small unmanned aerial vehicle (suav). *IEEE Dataport*, 2022.

[7] G. Galati. *100 Years of Radar*. Springer International Publishing, 2016.

[8] M.I. Skolnik. *Introduction to Radar Systems*. Electrical engineering series. McGraw-Hill, 2001.

[9] Tapan K. Sarkar and Magdalena Salazar Palma. A history of the evolution of radar. In *2014 44th European Microwave Conference*, pages 734–737, 2014.

[10] Christian Huelsmeyer, the inventor. `http://www.radarworld.org/huelsmeyer.html`. Accessed on: 27-03-2023.

[11] Niraj Bhatta and Geetha Priya .M. Radar and its applications. *International Science Press*, 10:1–9, 01 2017.

[12] M.A. Richards. *Fundamentals of Radar Signal Processing, Second Edition*. McGraw-Hill Education, 2014.

[13] M.I. Skolnik. *Radar Handbook, Third Edition*. Electronics electrical engineering. McGraw-Hill Education, 2008.

[14] H. Meikle. *Modern Radar Systems*. Artech House radar library. Artech House, 2008.

[15] Adam Johansson. Phased array system toolbox: An implementation of radar system. Faculty of Health, Science and Technology, April 2018.

[16] M.C. Budge and S.R. German. *Basic Radar Analysis, Second Edition*. Artech House radar library. Artech House, 2020.

[17] Hsueh-Jyh Li and Yean-Woei Kiang. 10 - radar and inverse scattering. In WAI-KAI CHEN, editor, *The Electrical Engineering Handbook*, pages 671–690. Academic Press, Burlington, 2005.

[18] Ke Pang, Yongjun Xie, Legen Dai, and Peiyu Wu. Design of ultra high aperture efficiency surface wave antenna array based on the three-dimensional aperture principle. *Electronics*, 11(21), 2022.

[19] H. Deng and Z. Geng. *Radar Networks*. CRC Press Taylor & Francis Group, 2020.

[20] B.R. Mahafza. *Radar Systems Analysis and Design Using MATLAB (Third Edition)*. Taylor & Francis, 2005.

[21] Xinyue Wang. Design of the frequency modulated continuous wave (fmcw) waveforms, simulation of the real road scenario and signal processing for the automotive adaptive cruise control. In *2021 IEEE International Conference on Power Electronics, Computer Applications (ICPECA)*, pages 815–830, 2021.

[22] Radar processing - the radar cube. `https://www.renesas.com/us/en/blogs/basics-fmcw-radar`.

[23] S.Z. Gurbuz. *Deep Neural Network Design for Radar Applications*. Radar, Sonar and Navigation. Institution of Engineering and Technology, 2020.

[24] N. Kehtarnavaz and N. Kim. *Digital Signal Processing System Design: LabVIEW-Based Hybrid Programming*. Digital Signal Processing SET. Elsevier Science, 2008.

[25] Pardhu Thottempudi, Kavya Sree, and K Tanuja. Design of matched filter for radar applications. In *International Conference on Circuits And Systems (CIRSY2014)*, 10 2014.

[26] Tyler Ridder and Ram Narayanan. Operational reliability of a moving target indication (mti) radar. In *Radar Sensor Technology XXIV*, page 4, 04 2020.

[27] K.J. Anderson, J. Ward, and R.M. O'Donnell. Adaptive doppler filtering applied to modern air traffic control radars. In *Proceedings of the 2004 IEEE Radar Conference (IEEE Cat. No.04CH37509)*, pages 242–248, 2004.

[28] R. Klemm, Institution of Engineering, and Technology. *Principles of Space-Time Adaptive Processing*. IET radar, sonar, navigation and avionics series. Institution of Engineering and Technology, 2006.

[29] A. Maio and Maria Greco. *Modern Radar Detection Theory*. Scitech Publishing, 01 2016.

[30] Maria-Pilar Jarabo-Amores, David Mata-Moya, Roberto Gil-Pita, and Manuel Rosa-Zurera. Radar detection with the neyman-pearson criterion using supervised-learning-machines trained with the cross-entropy error Emerging radar techniques. *EURASIP Journal on Advances in Signal Processing*, 2013, 12 2013.

[31] Jozef Perdoch, Stanislava Gažovová, Miroslav Pacek, Zdeněk Matoušek, and Ján Ochodnický. CFAR Algorithm for Improving Detections on Radar Raw Data Matrices. In *2022 New Trends in Signal Processing (NTSP)*, pages 1–6, 2022.

[32] Anil Chepala, Vincent Fusco, Umair Naeem, and Adrian McKernan. Uniform linear antenna array beamsteering based on phase-locked loops. *Electronics*, 12(4), 2023.

[33] C.A. Balanis. *Antenna Theory: Analysis and Design*. Wiley, 2015.

[34] B. Friedlander. The mythical uniform linear antenna array. In *2021 55th Asilomar Conference on Signals, Systems, and Computers*, pages 221–225, 2021.

[35] S. Bhuiya, F. Islam, and Mohammad Matin. Analysis of direction of arrival techniques using uniform linear array. *International Journal of Computer Theory and Engineering*, 4:931–934, 01 2012.

[36] Jacob Benesty, Jingdong Chen, and Yiteng Huang. *Microphone Array Signal Processing*, volume 125. Springer Berlin, Heidelberg, 04 2008.

[37] Radar Data Cube Concept. `https://www.mathworks.com/help/phased/gs/radar-data-cube.html`.

[38] Zhe Geng, He Yan, Jindong Zhang, and Daiyin Zhu. Deep-learning for radar: A survey. *IEEE Access*, 9:141800–141818, 2021.

[39] Rikiya Yamashita, Mizuho Nishio, Richard Kinh Gian Do, and Kaori Togashi. Convolutional neural networks: an overview and application in radiology. *Insights into Imaging*, 9:611–629, 08 2018.

[40] P. Kim. *MATLAB Deep Learning: With Machine Learning, Neural Networks and Artificial Intelligence*. Apress, 2017.

[41] Raghuram Vadlamani and Anjali Patel. Deep convolutional net, 03 2021.

[42] Qifan Pu, Sidhant Gupta, Shyamnath Gollakota, and Shwetak Patel. Whole-home gesture recognition using wireless signals. In *Proceedings of the 19th Annual International Conference on Mobile Computing and Networking*, MobiCom '13, page 27–38, New York, NY, USA, 2013. Association for Computing Machinery.

[43] Yan Wang, Jian Liu, Yingying Chen, Marco Gruteser, Jie Yang, and Hongbo Liu. E-eyes: Device-free location-oriented activity identification using fine-grained wifi signatures. In *Proceedings of the 20th Annual International Conference on Mobile Computing and Networking*, MobiCom '14, page 617–628, New York, NY, USA, 2014. Association for Computing Machinery.

[44] Sizhe An and Umit Y. Ogras. Mars: Mmwave-based assistive rehabilitation system for smart healthcare. *ACM Trans. Embed. Comput. Syst.*, 20(5s), sep 2021.

[45] Shelly Vishwakarma, Wenda Li, Chong Tang, Karl Woodbridge, Raviraj Adve, and Kevin Chetty. Simhumalator: An open source wifi based passive radar human simulator for activity recognition, 2021.

[46] Pedestrian and Bicyclist Classification Using Deep Learning. `https://www.mathworks.com/help/radar/ug/pedestrian-and-bicyclist-classification-using-deep-learning.html`.

[47] Backscatter radar signals from pedestrian. `https://www.mathworks.com/help/radar/ref/backscatterpedestrian.html`.

[48] Backscatter radar signals from bicyclist. `https://www.mathworks.com/help/radar/ref/backscatterbicyclist.html`.

[49] H.C. Yildirim, L. Storrer, M. Van Eechkhaute, C. Desset, J. Louveaux, and F. Horlin. Passive radar based on 802.11ac signals for indoor object detection. In *2019 16th European Radar Conference (EuRAD)*, pages 153–156, 2019.

[50] Antonios Argyriou. Obfuscation of human micro-doppler signatures in passive wireless radar. *IEEE Access*, 11:40121–40127, 2023.

[51] J.G. Proakis and M. Salehi. *Communication Systems Engineering*. Pearson Education. Prentice Hall, 2002.

[52] What Is the Average Walking Speed of an Adult? `https://www.healthline.com/health/exercise-fitness/average-walking-speed#average-speed-by-age`.

[53] Ben Marinberg, Ariel Cohen, Eilam Ben-Dror, and Haim H. Permuter. A study on mimo channel estimation by 2d and 3d convolutional neural networks. In *2020 IEEE International Conference on Advanced Networks and Telecommunications Systems (ANTS)*, pages 1–6, 2020.

[54] Wenda Li, Mohammud Junaid Bocus, Chong Tang, Robert J. Piechocki, Karl Woodbridge, and Kevin Chetty. On csi and passive wi-fi radar for opportunistic physical

activity recognition. *IEEE Transactions on Wireless Communications*, 21(1):607–620, 2022.